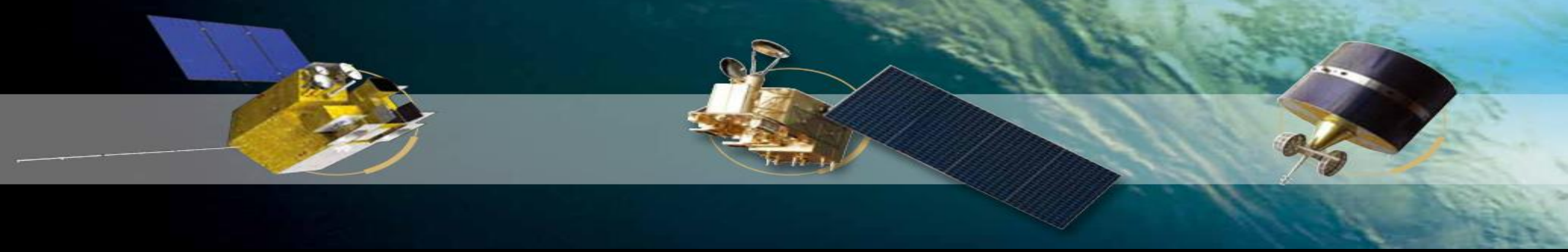

Tropopause folds measured by Fengyun-4: Preliminary validation and their relation to hazard weather events

SHOU Yi-Xuan, Lu Feng, Wang Sixian

National Satellite of Meterorological Center,
Chinese Meterological Administration

AOMSUC-12, 11-18 Nov. 2022, Japan

shouyx@cma.gov.cn

Outline

1. Background and Motivation

- **Climate distribution of tropopause**

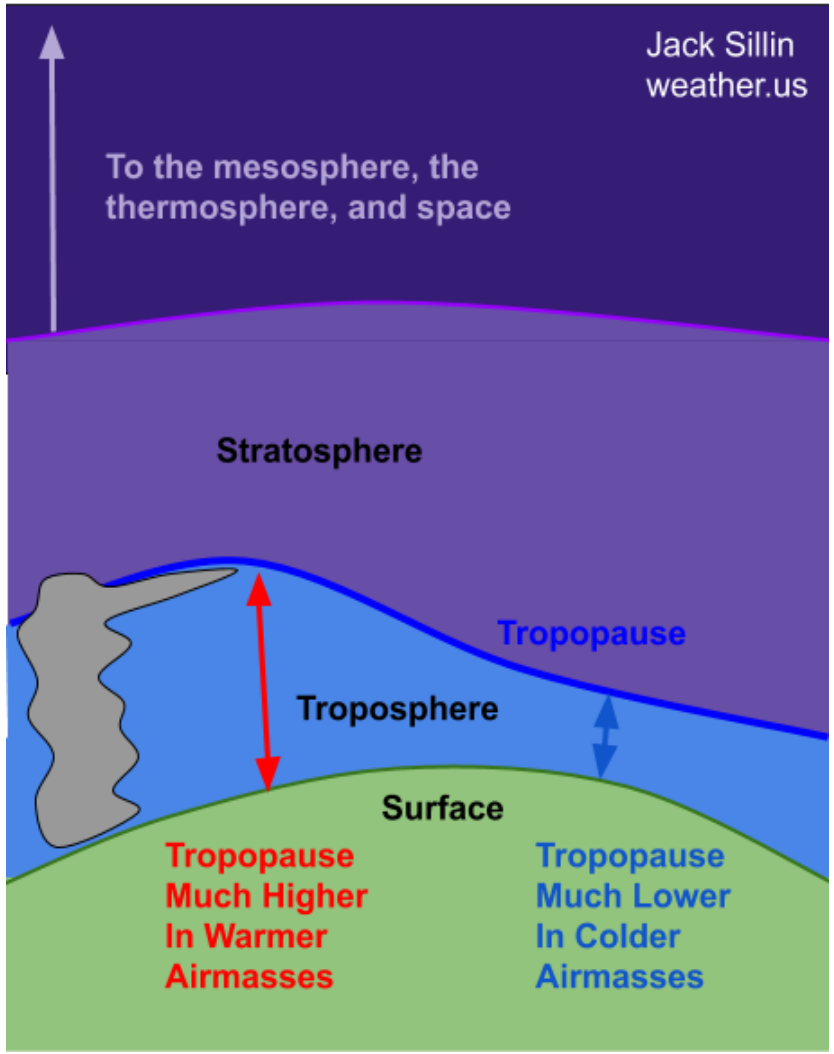

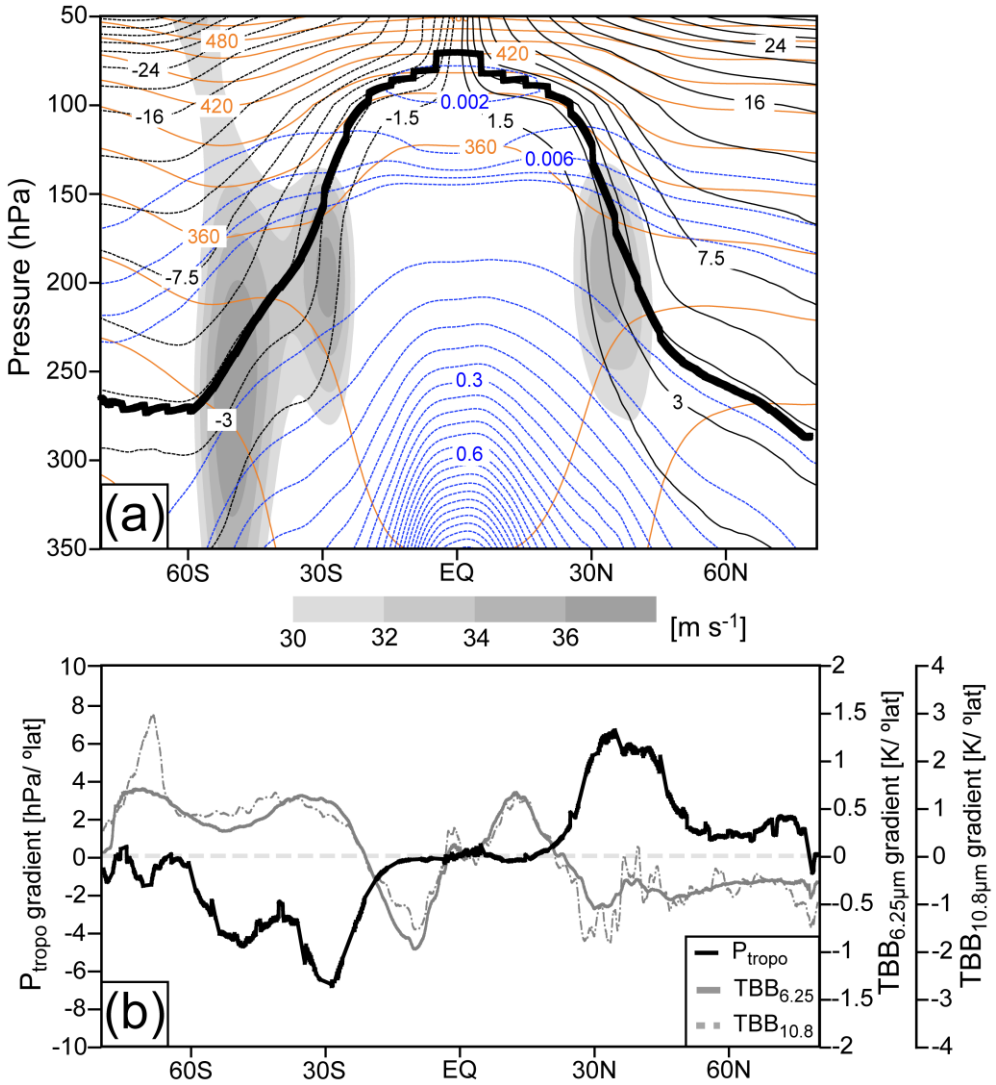

1. Background and Motivation

➢ Porperties of tropopause

$PV = \sigma^{-1}\zeta_a$: potential vorticity (Unit: PVU=10^{-6} m^2 s^{-1} K kg^{-1})

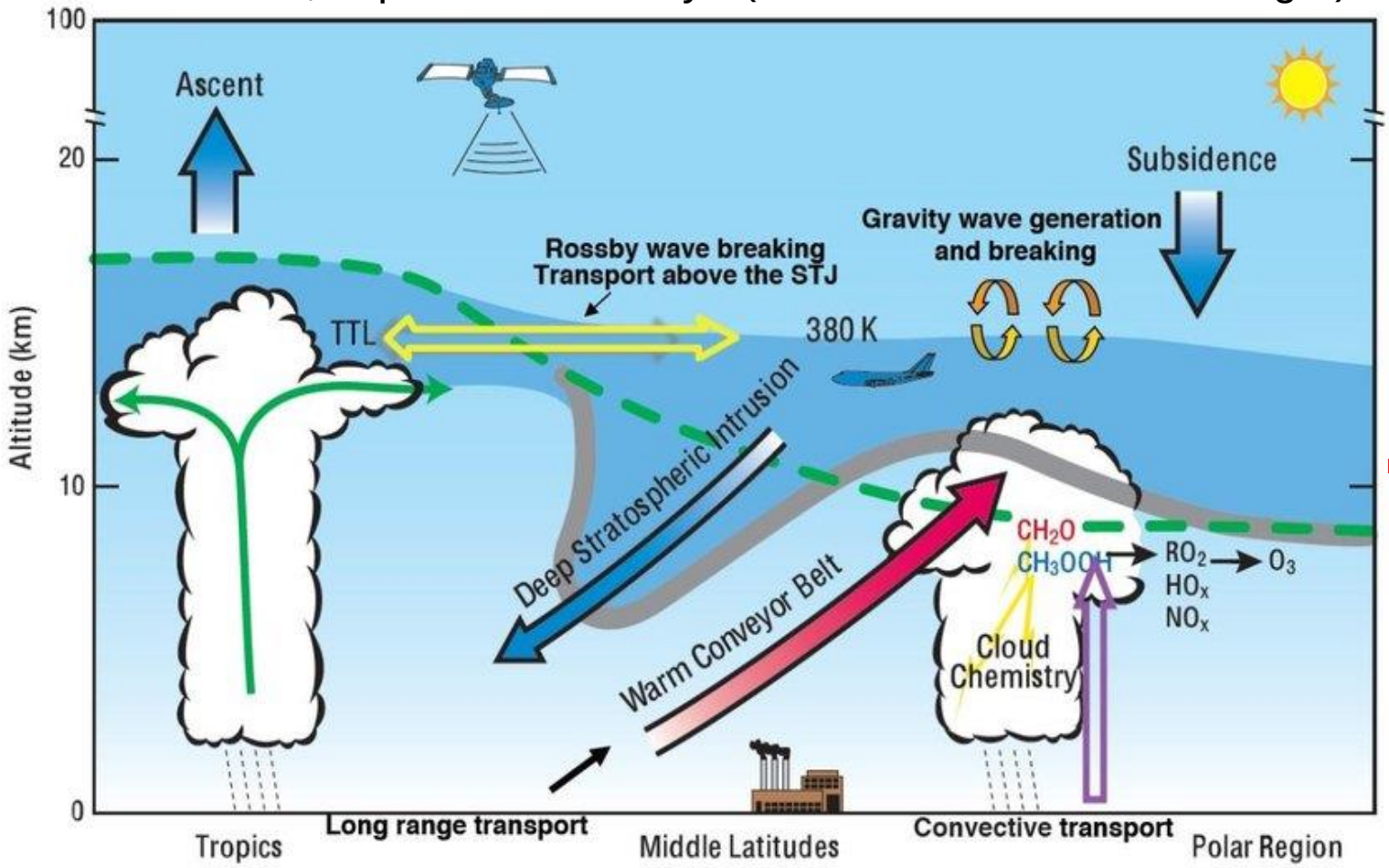

In the stratosphere PV > 3 PVU , due to the strong increase of the static stability.

tropopause --"valve"

In the middle and upper troposphere PV is ranging from 0.5 to 1 PVU

The surface of constant PV = 2 PVU is defined as the "dynamical tropopause" .

1. Background and Motivation

➢ Tropopause foldings

A local minimum of the 2 PVU surface height is tropopause dynamic anomaly which is commonly called as “tropopause folding”. It is often shown as a funnel in vertical.

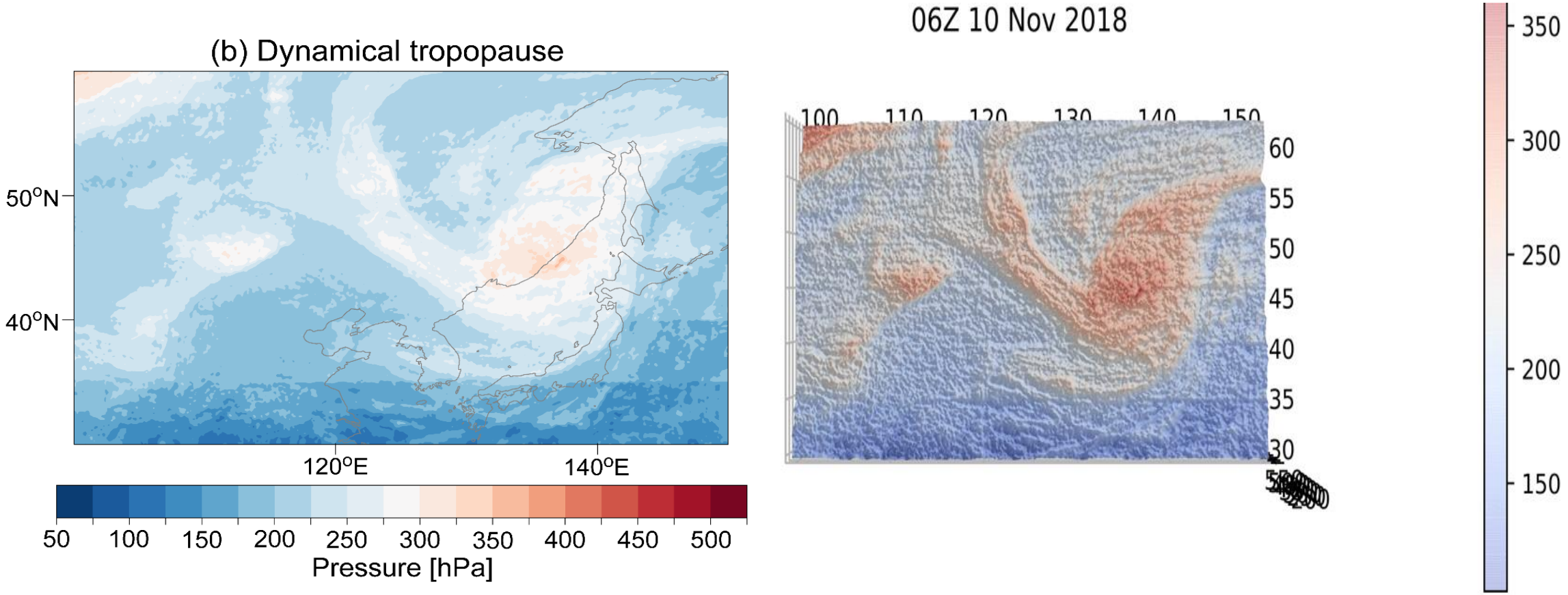

Figure. The 2-D and 3-D views of the dynamcial tropopause and “tropopause folding” in vertical.

1. Background and Motivation

➢ Porperties of tropopause

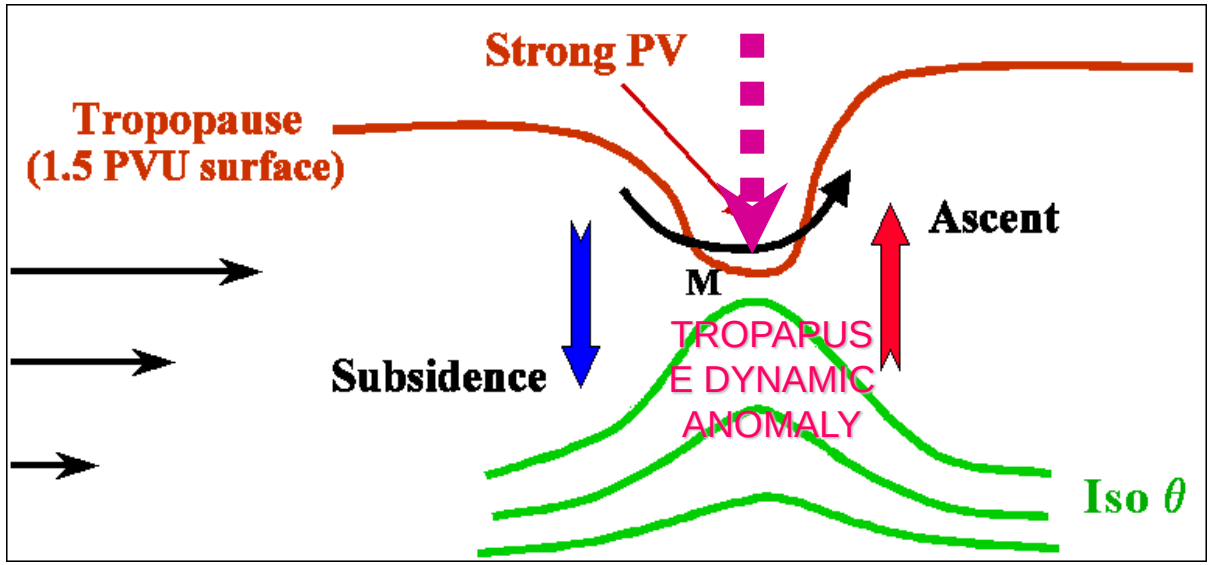

Through this “funnel” , air masses from stratosphere which are dry and having a high PV can enter into troposphere. Due to the PV conservation, the anomaly may lead to deformations in θ and vorticity of the surrounding air, which will induce the gensis of cyclone, kata- and ana-cold fronts,sometimes may also stimulate local convective weather.

Although tropopause foldings have close relationship with weather and climate change, so far they are mainly calculated by numerical models, and a few by radar observations. While a wide range of their spatial distributions obtained from observations is not available yet. According to previous study this phenomenon can be observed by some channels on satellite. As documented, they often exhibit as dark grey shades in WV channel images (Santurette and Georgiev, 2005).

1. Background and Motivation

➢ **Fengyun-4 -- The new generation geostationary satellite of China**

- Fengyun-4A: launched in Dec. 2016
- Fengyun-4B: launched in Jun. 2021

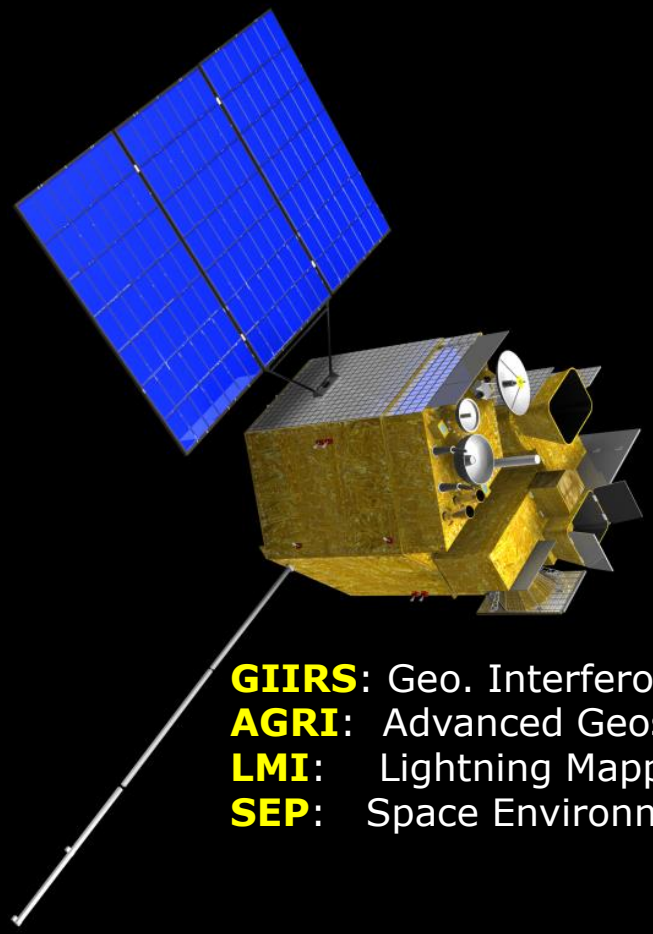

1. Launch Weight: approx 5300kg
2. Stabilization: Three-axis
3. Attitude accuracy: 3″
4. Bus: 1553B+Spacewire
5. Raw data transmission : X band
6. Output power: >= 3200W
7. Design life: over 7 years

GIIRS: Geo. Interferometric Infrared Sounder
AGRI: Advanced Geosynchronous Radiation Imager
LMI: Lightning Mapping Imager
SEP: Space Environment Package

1. Background and Motivation

FY-4 AGRI

Channels		Wavelength (μm)	Spatial resolution(km)	Main Application
VIS & Near-Infrared	1	0.45-0.49	1.0	Aerosol
	2	0.55-0.75	0.5-1.0	Fog, Clound
	3	0.75-0.90	1.0	Vegetation
Short-wave Infrared	4	1.36-1.39	2.0	Cirrus
	5	1.58-1.64	2.0	Cloud,Snow
	6	2.1-2.35	2.0-4.0	Cirrus,Aerosol
Mid-wave Infrared	7	3.5-4.0(High)	2.0	Fire
	8	3.5-4.0(Low) *	4.0	Land surface
Water Vapor	9	5.8-6.7	4.0	water vapor within upper troposphere
	10	6.9-7.1	4.0	water vapor within middle troposphere
	11	7.3-7.5	4.0	water vapor within low troposphere
Long-wave infrared	12	8.0-9.0	4.0	water vapor within low troposphere,cloud
	13	10.3-11.3	4.0	Window channel,cloud top height
	14	11.5-12.5	4.0	Window channel,cloud top height
	15	13.2-13.8	4.0	CO2 channel, cloud top height

1. Background and Motivation

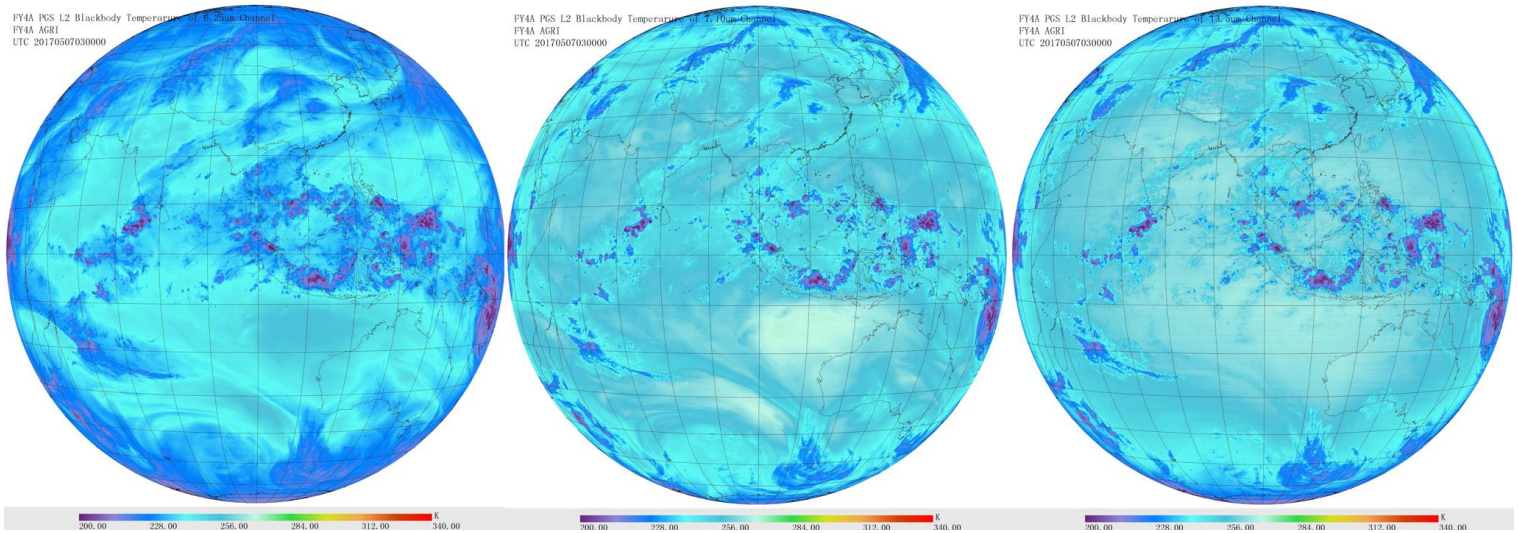

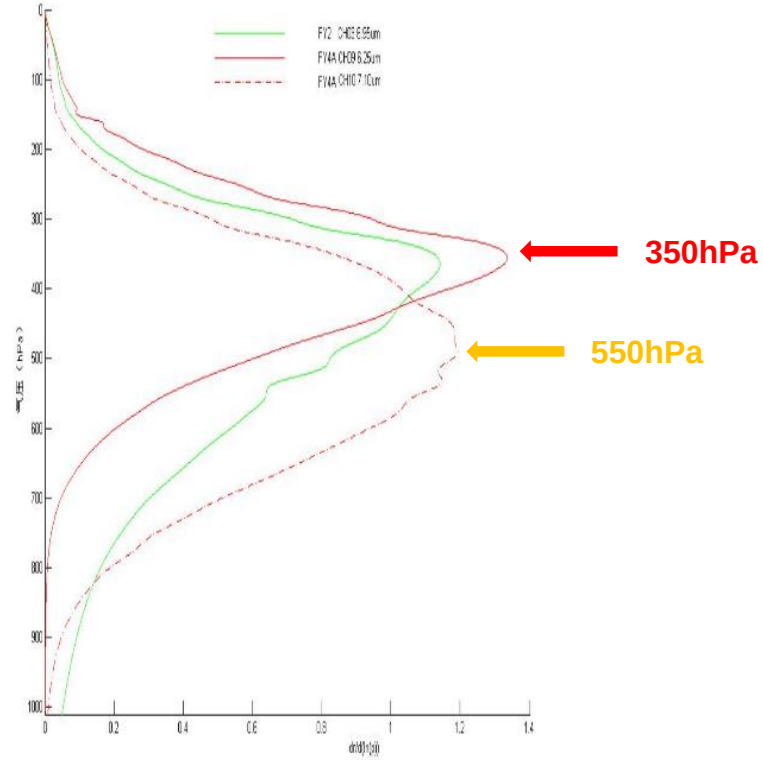

Sensitive to water vapor variation within mid to upper troposphere!!

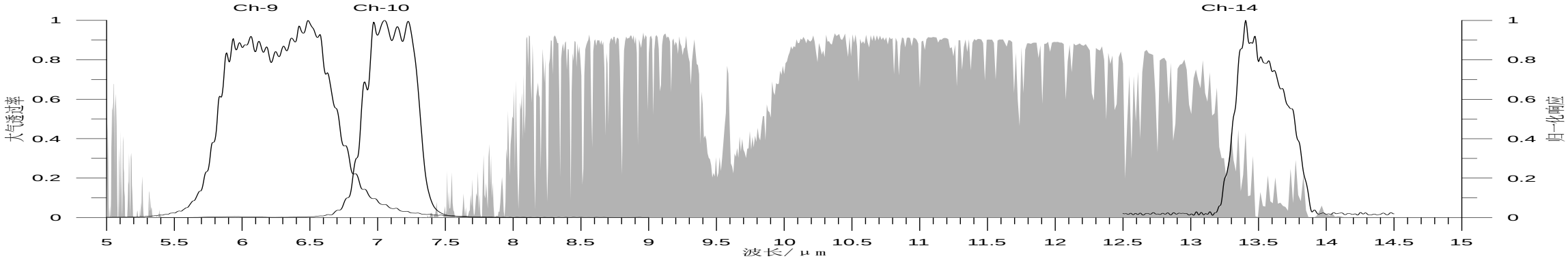

1. Background and Motivation

- **Relationships between tropopause foldings and Fengyun-4B observations**

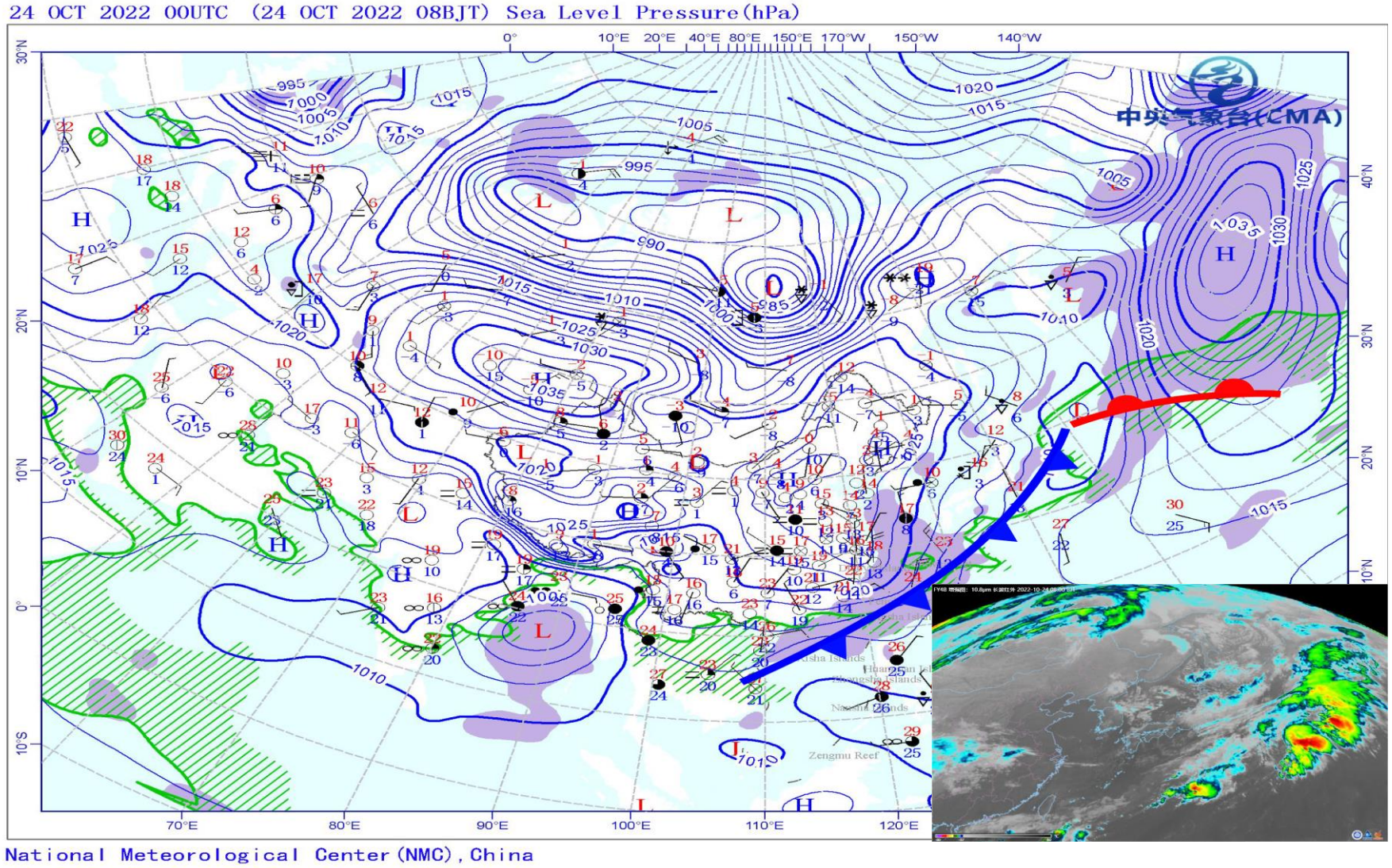

Figure. Surface weather map on 0000UTC Oct. 24, 2022 (Adapted from Chinese meteorological center) (blue solid lines are surface pressure; green hash lines are warm moist area; blue thick solid lines with blue triangles indicate cold front; while red thick solid lines with hemicircles are warm front) (the cloud image on the bottom right corner is Fengyun-4B 10.8μm enhance cloud image at the same time as the surface weather map)

1. Background and Motivation

Airmass RGB

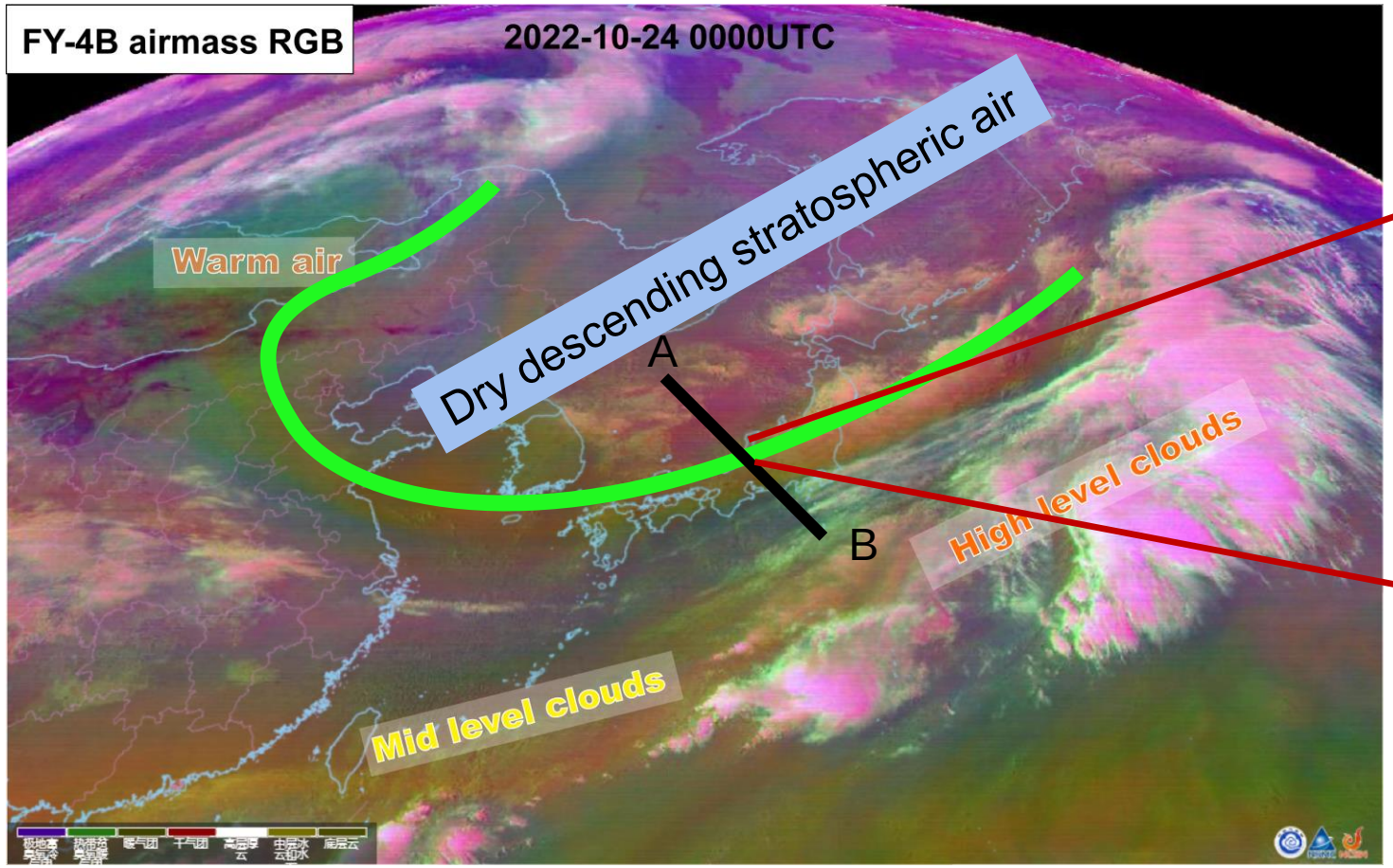

Note: **brown** to **purple**: dry descending stratopsheric air
earth yellow : mid level clouds
pink : high level clouds

Figure. Fengyun-4B airmass RGB product on 0000UTC Oct. 24, 2022

FY-4B Enhanced WV 6.2μm channel

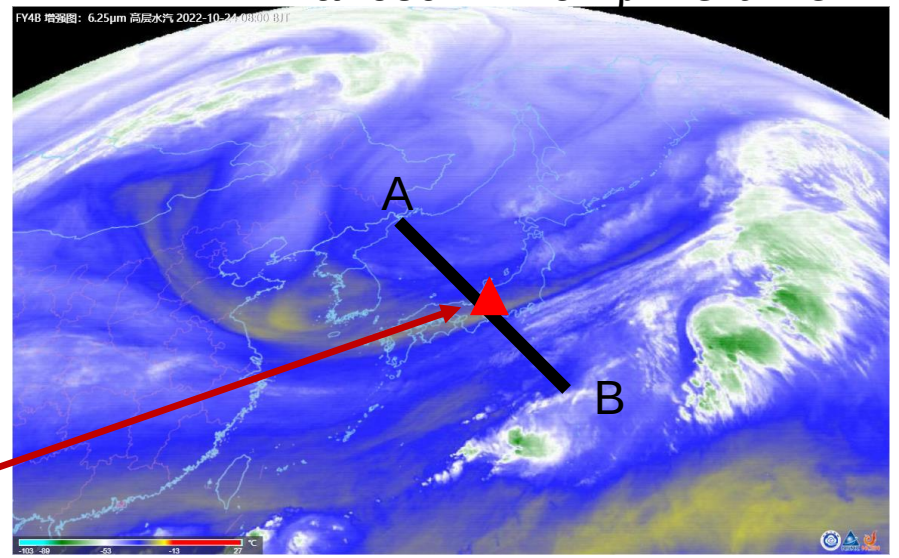

Note: **yellow** to **red**: high brightness temperature (dry)
blue to **green**: low brightness temperature (moist)

FY-4B Enhanced WV 6.95μm channel

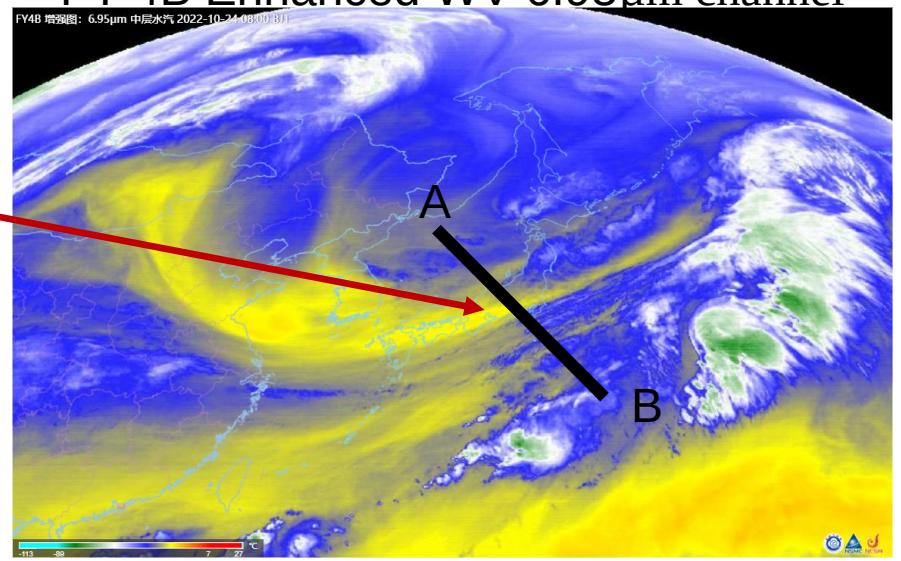

Figure. Fengyun-4B enhanced WV channels on 0000UTC Oct. 24,

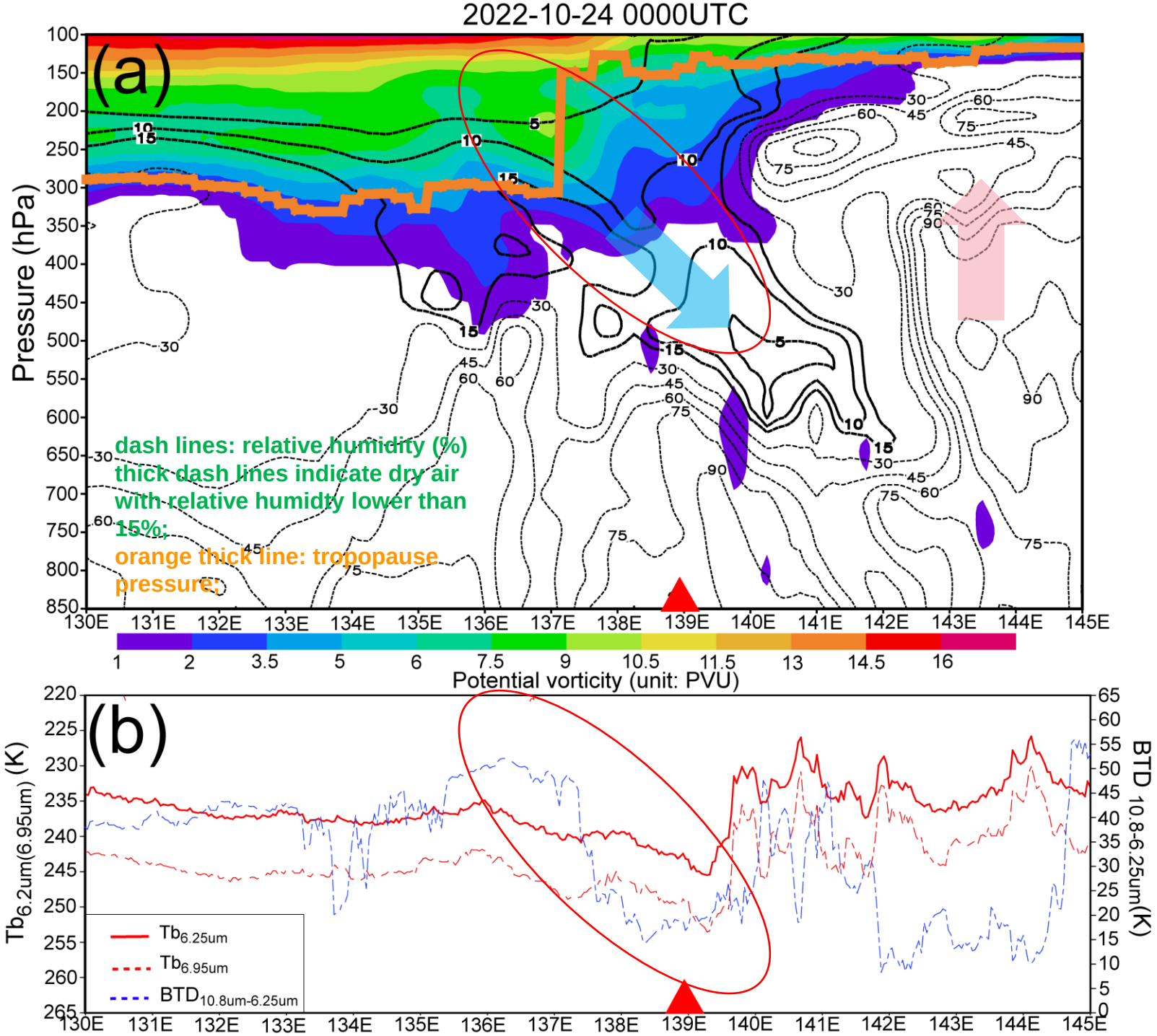

Downgliding dry and PV anomaly air correspond to the regions having:

- high brightness temperature in the upper and mid-level WV channels and low brightness temperature difference between the split-window channel (10.8μm) and upper-level WV channel (6.25μm);
- big horizontal gradients in tropopause height, brightness temperature of WV channels as well as the brightness temperature difference;

Figure. (a) Cross sections of potential vorticity (PV≧1PVU are color shaded)superposed by relative humidity (dash lines; thick dash lines indicate dry air with relative humidity lower than 15%) and tropopause height (orange thick line) along line AB. (b) FY-4B 6.25um,6.95um channels brightness temperature and brightness temperature difference between 10.8um and 6.25um along line AB. Blue arrow in figure (a) represents downdrafts and red arrow represents updrafts.

2. Scientific scheme

➢ Algorithm:

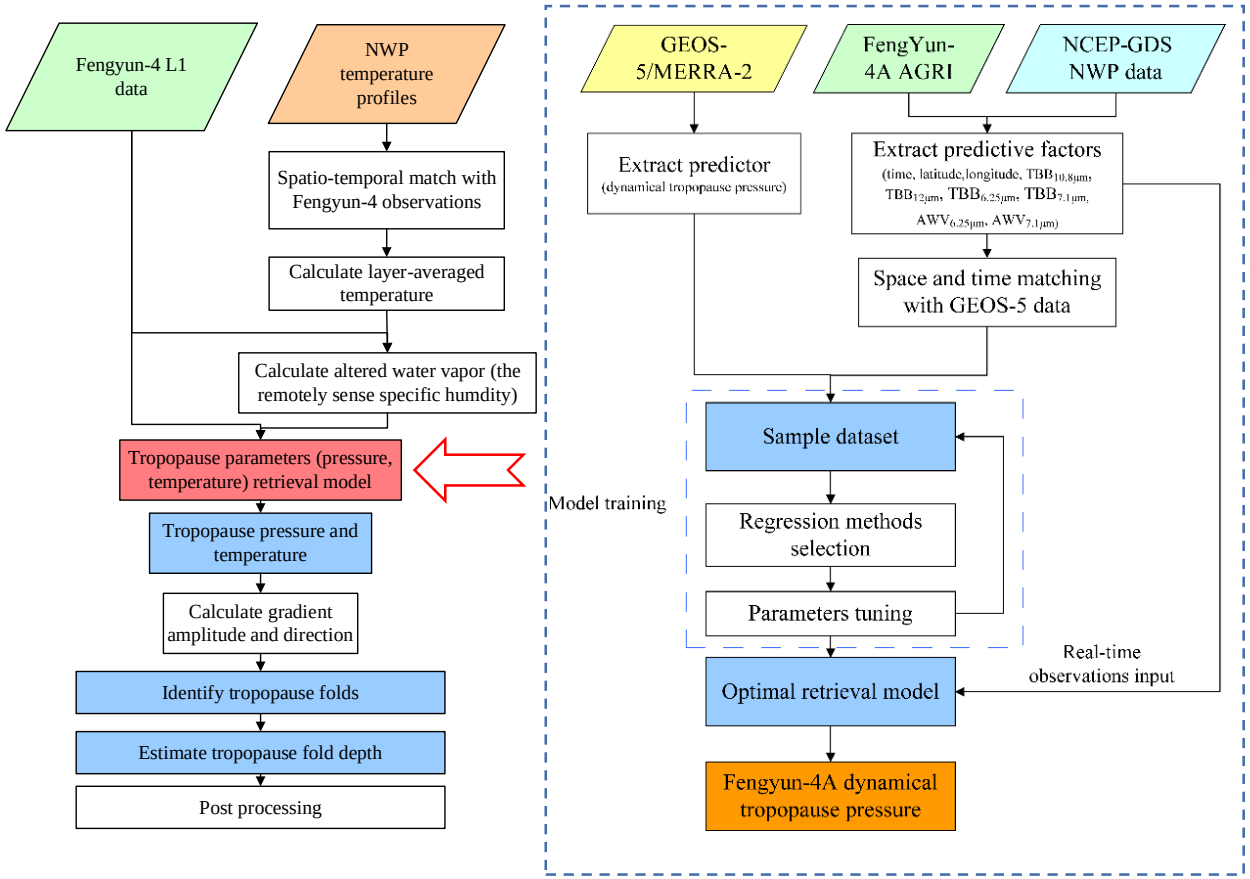

Figure. Flow chart of Fengyun-4 tropopause folding identification

Table. Input data for Fengyun-4 tropopause folding identification

Data used in the algorithm	Abbreviation	Definition	Main Application
Satellite observations	$Tb_{6.25\mu m}$	brightness temperature of 6.25μm channel (channel 9 of FY-4B)	water vapor within upper troposphere
	$Tb_{6.95\mu m}$	brightness temperature of 6.95μm channel (channel 10 of FY-4B)	water vapor within middle troposphere
	$Tb_{10.8\mu m}$	brightness temperature of 10.8 μm channel (channel 13 of FY-4B)	Window channel,cloud top height
	$Tb_{12.0\mu m}$	brightness temperature of 12.0 μm channel (channel 14 of FY-4B)	Window channel,cloud top height
NWP forecasting	$\overline{T}_{300-400hPa}$	layer averaged temperature within 300-400hPa	used with brightness temperature of 6.25μm channel for calculating psuedo water vapor at upper troposphere
	$\overline{T}_{500-600hPa}$	layer averaged temperature within 500-600hPa	used with brightness temperature of 6.95μm channel for calculating psuedo water vapor at middle troposhere

The whole algorithm include two parts:

- One is to set up a model for retrieving tropopause height (pressure) and temperature;
- The second is to identify tropopause foldings based on the retrieved tropopause parameters.
- The model for retrieving tropopause height (pressure) and temperature is established by the random forest method. The model is trained by using Fengyun-4 6.25μm, 6.95μm,10.8μm,12.0μm observations and a remotely sensed specific humidity (named as AWV, which is calculated based on Soden and Bretherton (1996) algorithm) as predictive parameters, and use tropopause parameters in GEOS-5/MERRA2 reanalysis data as predicted values.
- The algorithm for tropopause folding identificiation is then achieved by calculating the gradient amplitude and direction of the retrieved tropopause parameters (including tropopause pressure, temperature etc.) ;
- The preliminary results will be input into a post process system, which include a number of filting criteria for final optimization.

2. Scientific scheme

➢ Preliminary results：

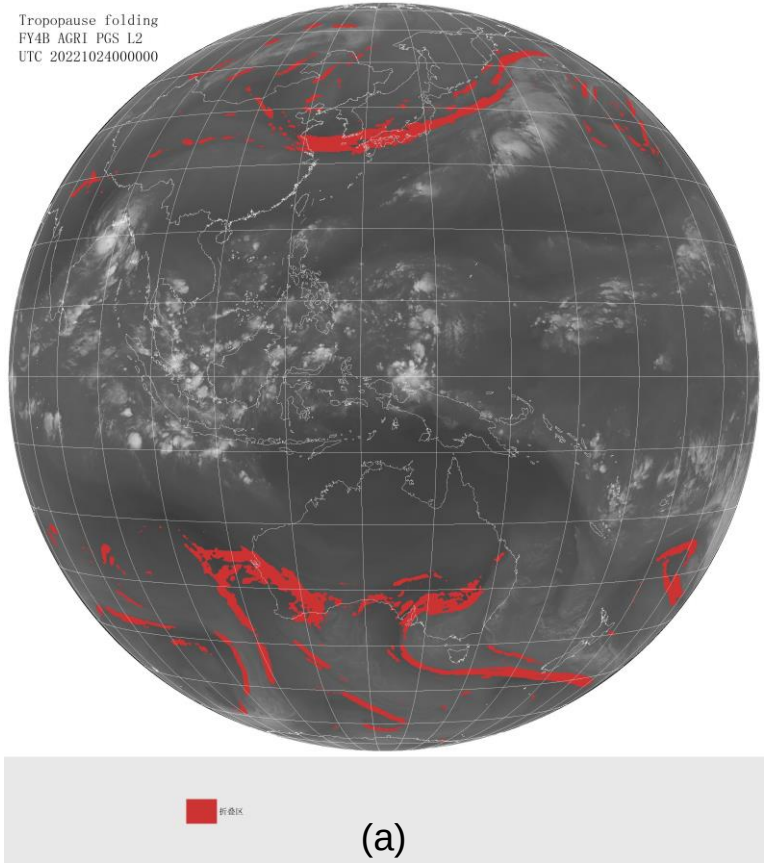

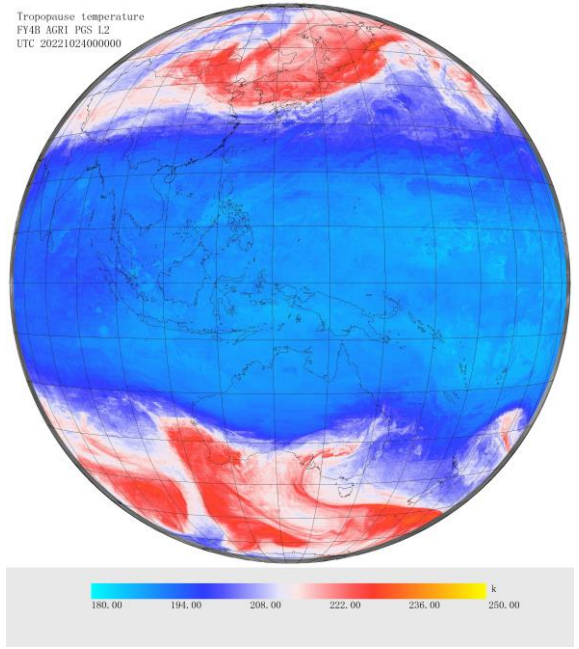

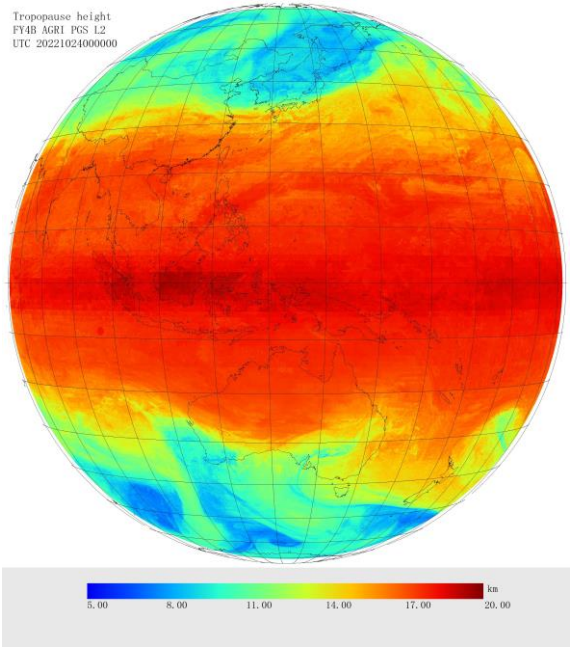

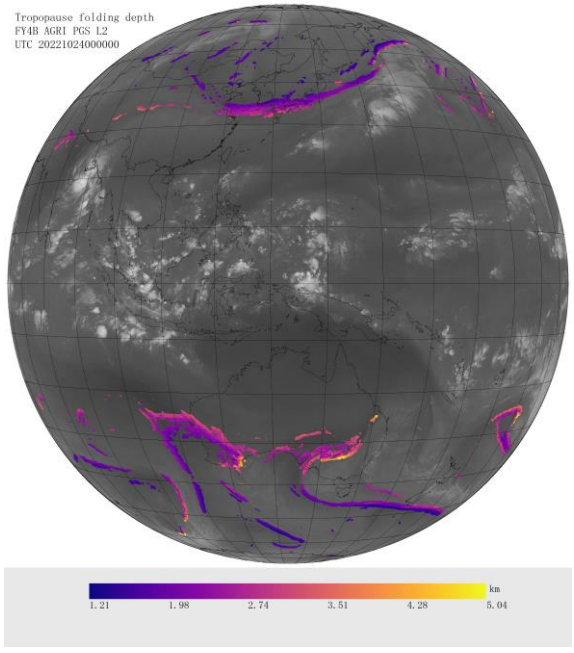

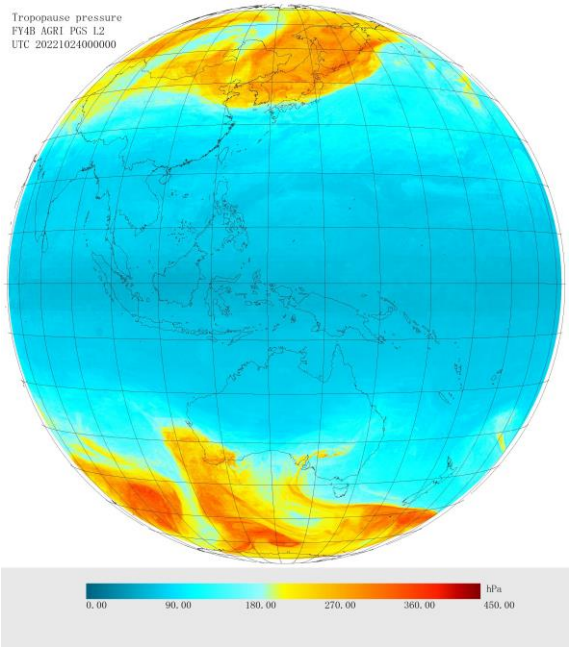

Figure. Preliminary results retrieved by the algorithm a) tropopause foldings (red shaded areas); b) tropopause temperature (Unit: K); c) tropopause height (unit: km); d) tropopause fold depth (unit: km); and e) tropopause pressure (unit: hPa) on 0000UTC Oct. 24, 2022.

3. Validation

➢ Data

GEOS-5/MERRA-2 reanalysis data:

☐ M2T1NXSLV dataset:

- temporal resolution of 1hr and a spatial resolution of 0.5× 0.625°

(refer to https://disc.gsfc.nasa.gov/datasets/M2T1NXSLV_5.12.4/summary?keywords=tropopause);

- used for the dynamical tropopause pressure and temperature validation;

☐ M2I3NPASM dataset:

- store the profiles of atmospheric parameters, such as wind, temperature and humidity;
- has 42 vertical levels;
- temporal resolution of 3 hr and a spatial resolution of 0.5× 0.625°;

(refer to https://disc.gsfc.nasa.gov/datasets/M2I3NPASM_5.12.4/summary?keywords=potential%20vorticity)

- used for tropopause foldings validation;

3. Validation

➢ Methods

a) Validation for tropopause pressure and temperature:

We use standard statistical methods for quantitatively evaluation.

$$\mathrm{MBE} = \frac{1}{N}\sum_{i=1}^{N} \emptyset_i^{'}, \quad (1)$$

$$\mathrm{RMSE} = \left[\frac{1}{N-1}\sum_{i=1}^{N} (\emptyset_i^{'})^2\right]^{1/2}, \quad (2)$$

$$\sigma = \left[\frac{1}{N}\sum_{i=1}^{N} (\emptyset_i^{'})^2\right]^{1/2}, \quad (3)$$

$$\mathrm{R} = \frac{\mathrm{Cov(X,Y)}}{\sigma_x \sigma_y} \quad (4)$$

- where X, Y represent the retrieval and the observed samples, respectively $\emptyset^{'}$ is the bias between a retrieval and an observation; σ_x is the standard deviation among the retrieval results, and $\mathrm{Cov(X,Y)}$ is the covariance between retrievals and observed samples. The MBE, RMSE and R represent the mean bias error, the root mean square error, and correlation coefficient, respectively.

3. Validation

➢ Methods

b) Validation for tropopause folding：

- tropopause foldings based on NWP data： The 3-D labeling method for tropopause folding identification method (Sprenger et al. 2003).

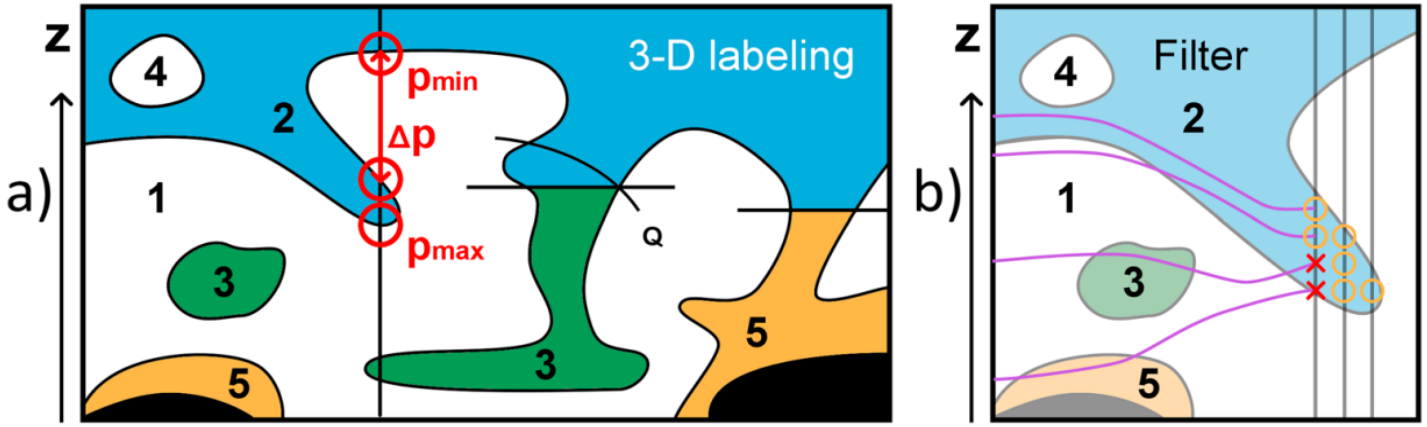

Figure. The 3-D labeling method for tropopause folding identification using NWP data (adapted from Sprenger et al. (2003))

3. Validation

➢ Methods

i) visual examination;

ii) quantitative validation：

To assess the skill of the algorithm by creating a set of 2 × 2 contingency tables and then comparing the satellite retrievals with the yes-or-no model results. The statistics indices used here are:

① Probability for identifying 'folds' by both two methods（POD_fold）;

② Probability for identifying 'no folds' (POD_unfold);

③ and the total hitting rate for the satellite retrievals relative to the model results (HR).

Table. Definition of the parameters used in the statistics

		FY-4B tropopause foldings	
		Y（have folds）	N（no folds）
NWP tropopause foldings	Y（have folds）	A(yy)	B(yn)
	N（no folds）	C(ny)	D(nn)

$$POD\_fold = \frac{A}{A+B} \tag{1}$$

$$POD\_unfold = \frac{D}{C+D} \qquad POD \in [0,1] \text{ ,} \tag{2}$$

$$HR = \frac{A+D}{A+B+C+D} \qquad HR \in [0,1] \text{ ,} \tag{3}$$

3. Validation

➢ Results

i) Tropopause pressure and temperature

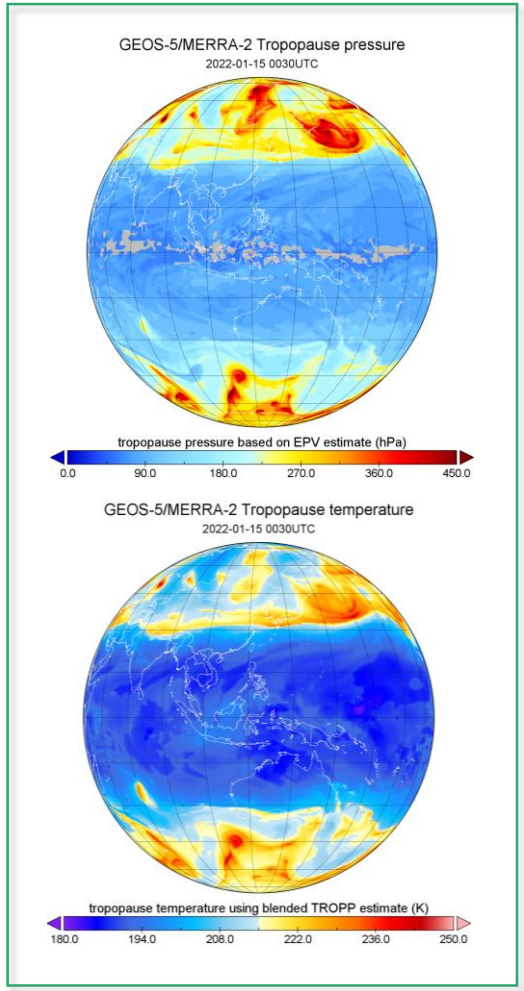

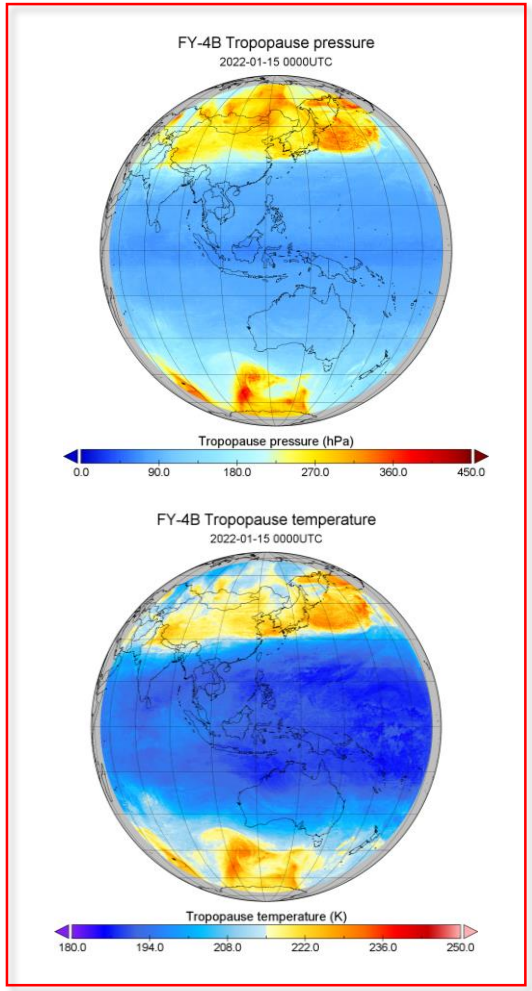

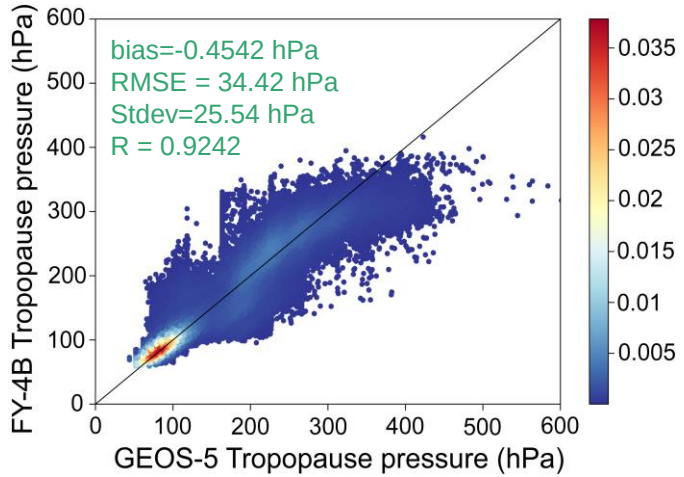

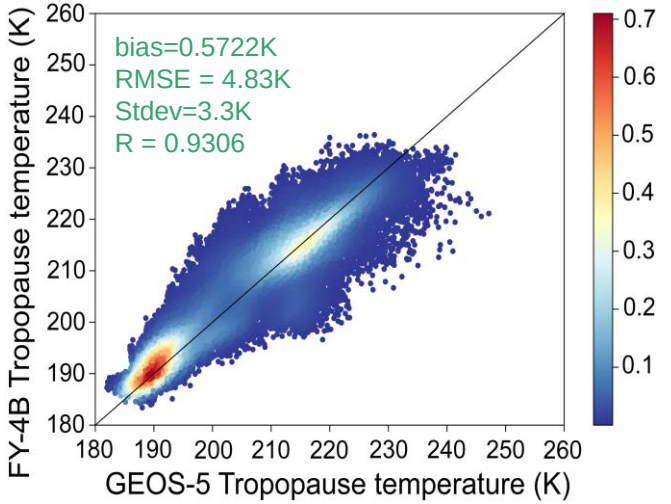

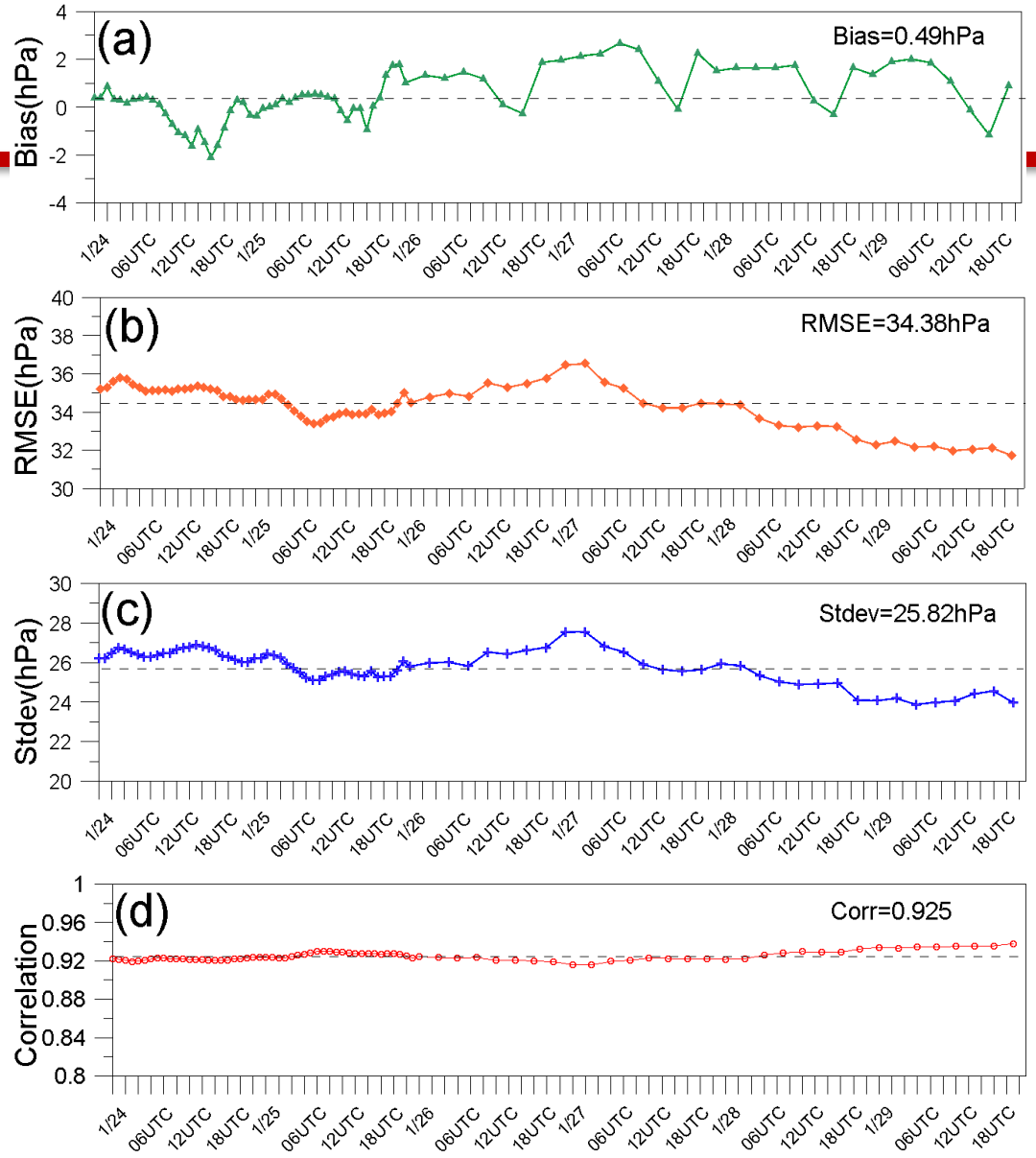

Figure. Validations against GEOS-5/MERRA-2 for FY-4B retrieved tropopause pressure during 24-29 Jan 2022 (total 144hrs) a) MBE; b) RMSE; c) Stddev; d) Correlation

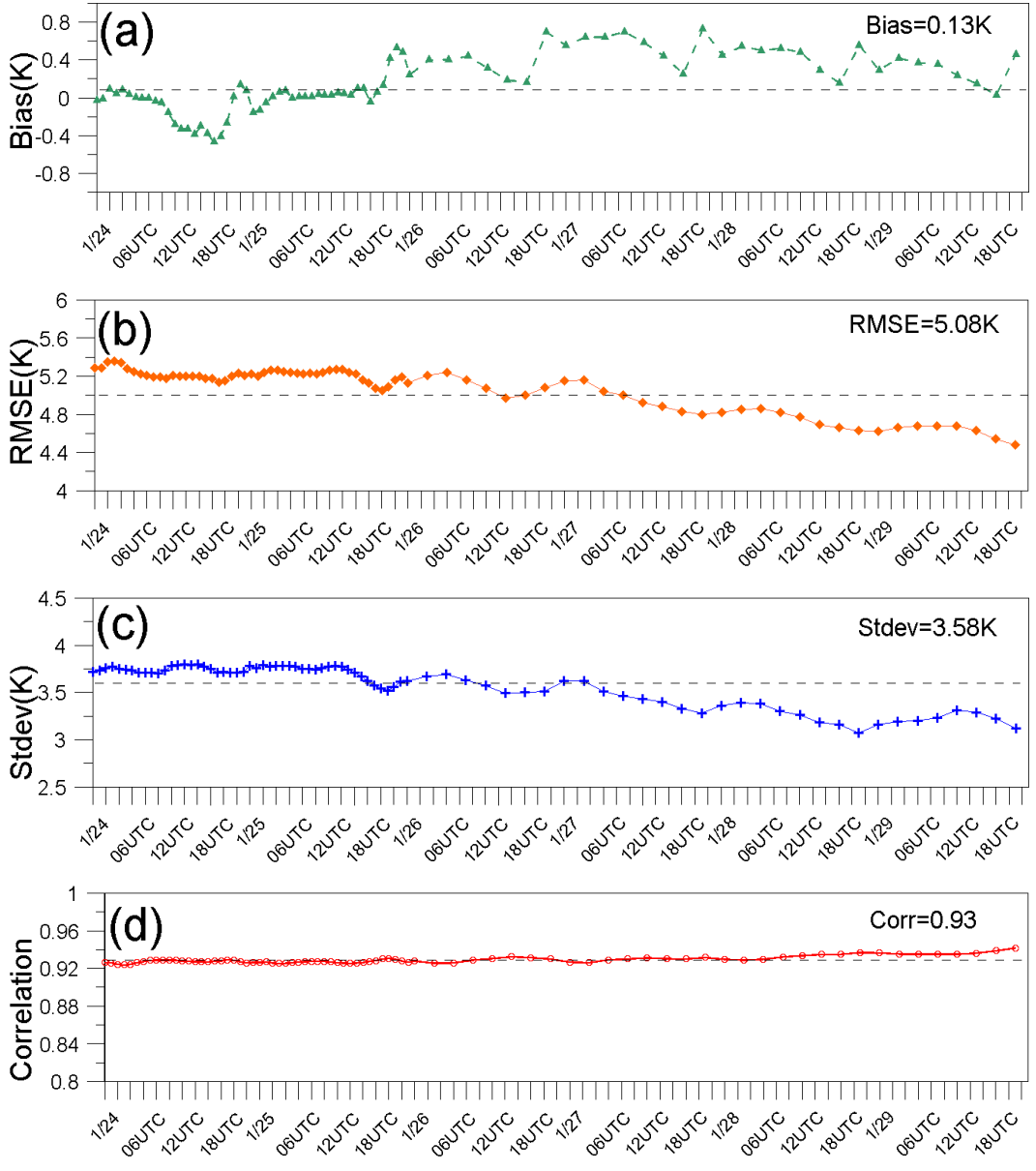

Figure. Validations against GEOS-5/MERRA-2 for FY-4B retrieved tropopause temperature during 24-29 Jan 2022 (total 144hrs) a) MBE; b) RMSE; c) Stddev; d) Correlation

3. Validation

➢ Results

ii) Tropopause folding:

GEOS-5/MERRA-2 Tropopause folds
2022-01-15 0000UTC

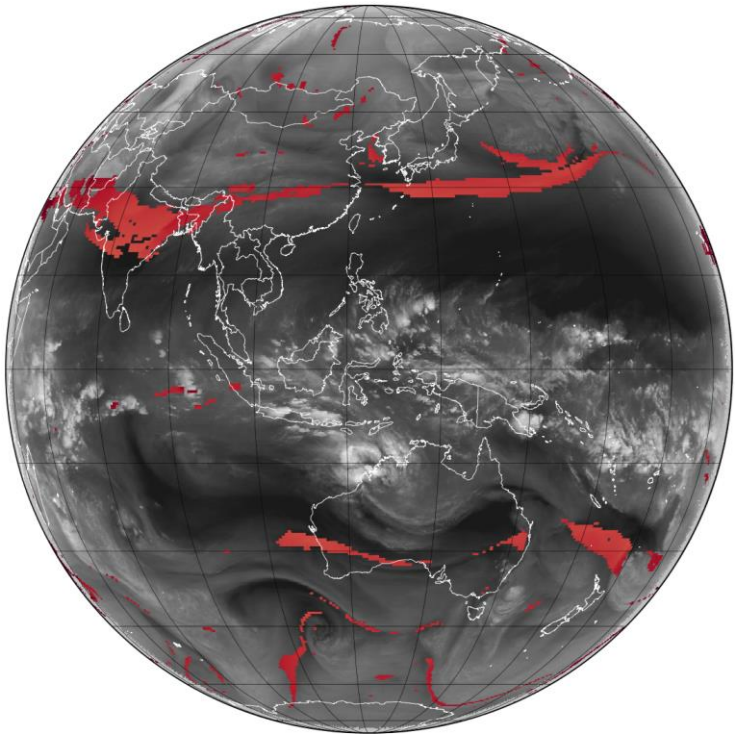

FY-4B Tropopause folding
2022-01-15 0000UTC

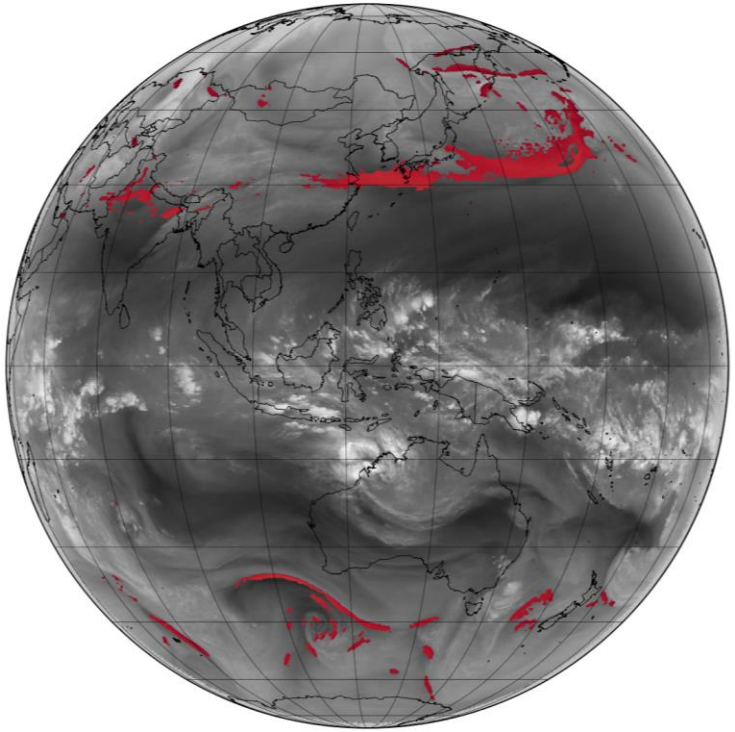

Tropopause Folding

Simple conceptual model

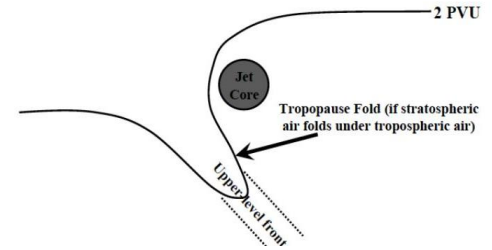

Upper level jets at 200 hPa
(from NCEP-FNL data)

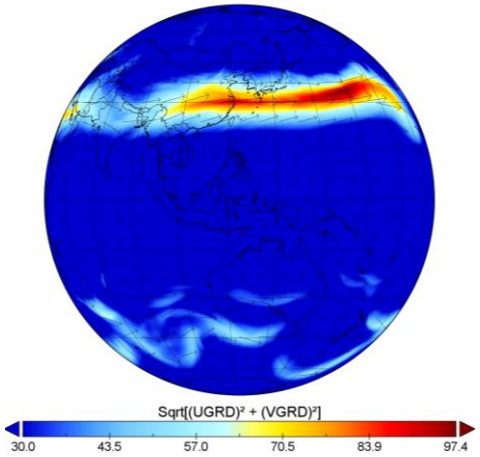

The spatial distributions of the tropopause foldings identified by NWP data and satellite observations are generally consistent. In the northern hemisphere, the tropopause foldings occur around 30° N, with the most concentrated area being over the sea area south to Japan. While in the southern hemisphere, the foldings are most seen over the sea area south to Australia. All the foldings corresponds to dark areas on the WV channel images and associate with upper level jets.

3. Validation

➢ Results

ii) Tropopause folding:

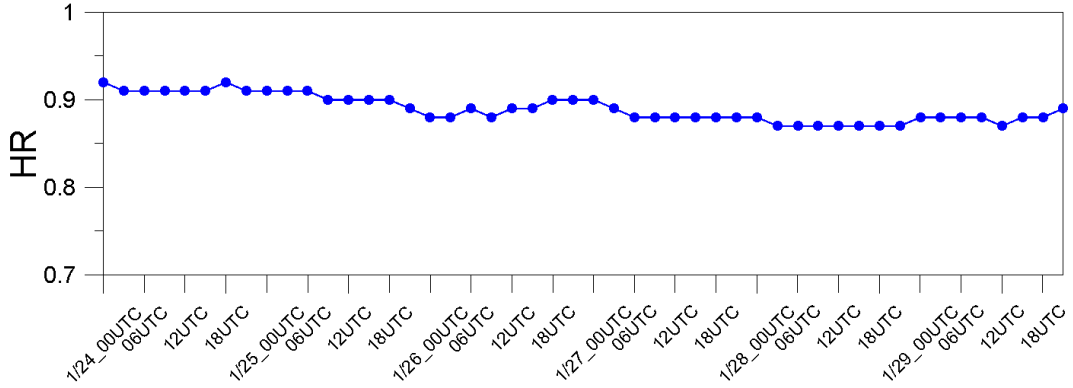

Figure. The hitting rates (HR) of FY-4B tropopause foldings during 24-29 Jan 2022 as compared to NWP tropopause foldings

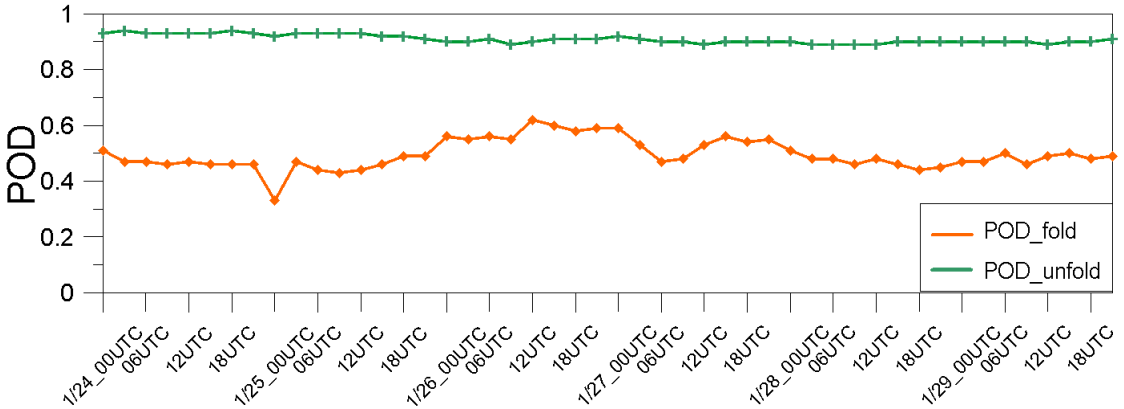

Figure. The probablity for identifying ‘folds’ and ‘unfold’ in FY-4B tropopause foldings and model results during 24-29 Jan 2022.

Valid samples： 1,862,448

Validations of FY-4B tropopause foldings
（compared to tropopause foldings identified by GEOS-5/MERRA-2 data using 3-D labeling method）

	FY4B tropopause foldings
HR	0.89
POD_fold	0.51
POD_unfold	0.91

4. Connection with hazard weather events

- **Indicate for the initiation of convections and cyclongensis**

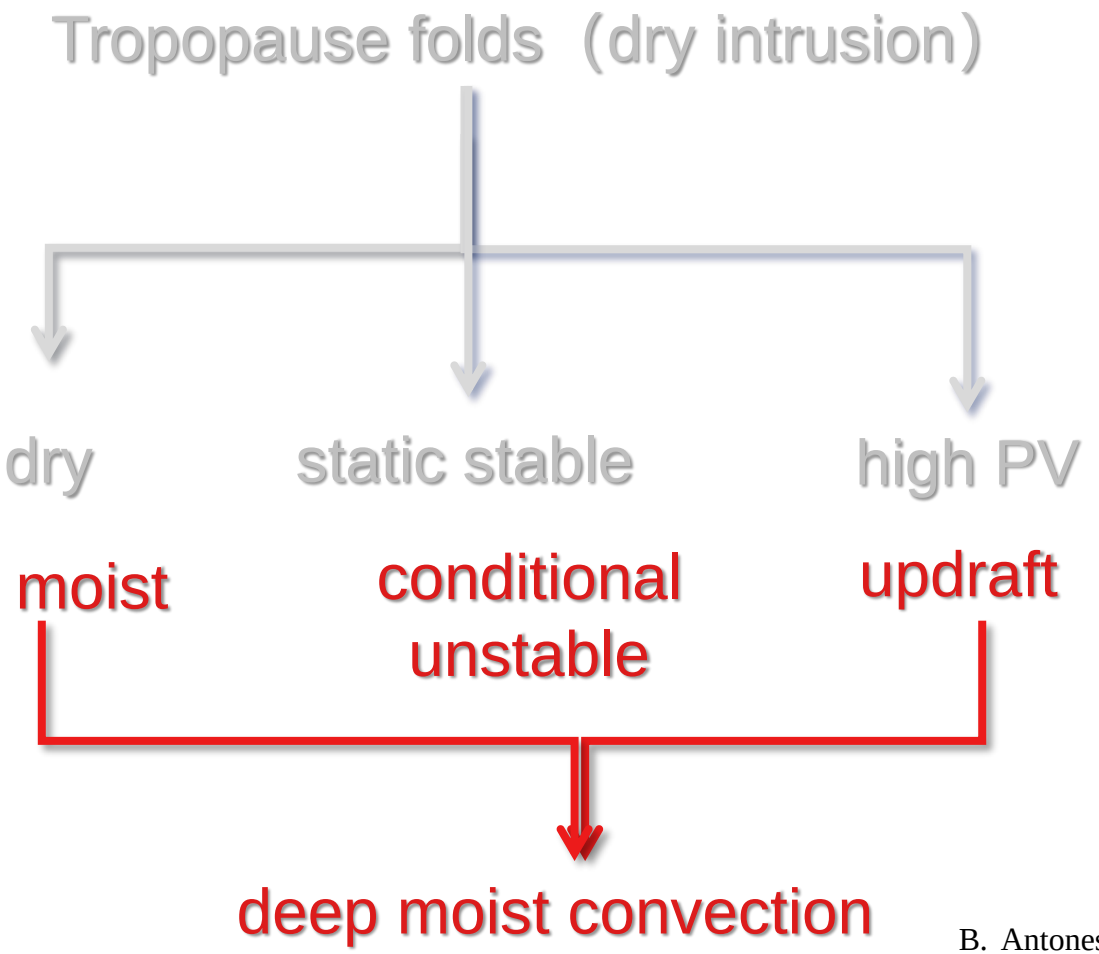

According to the statistics, almost 67% tropopause foldings occurred ahead of upper trough may trigger convection.

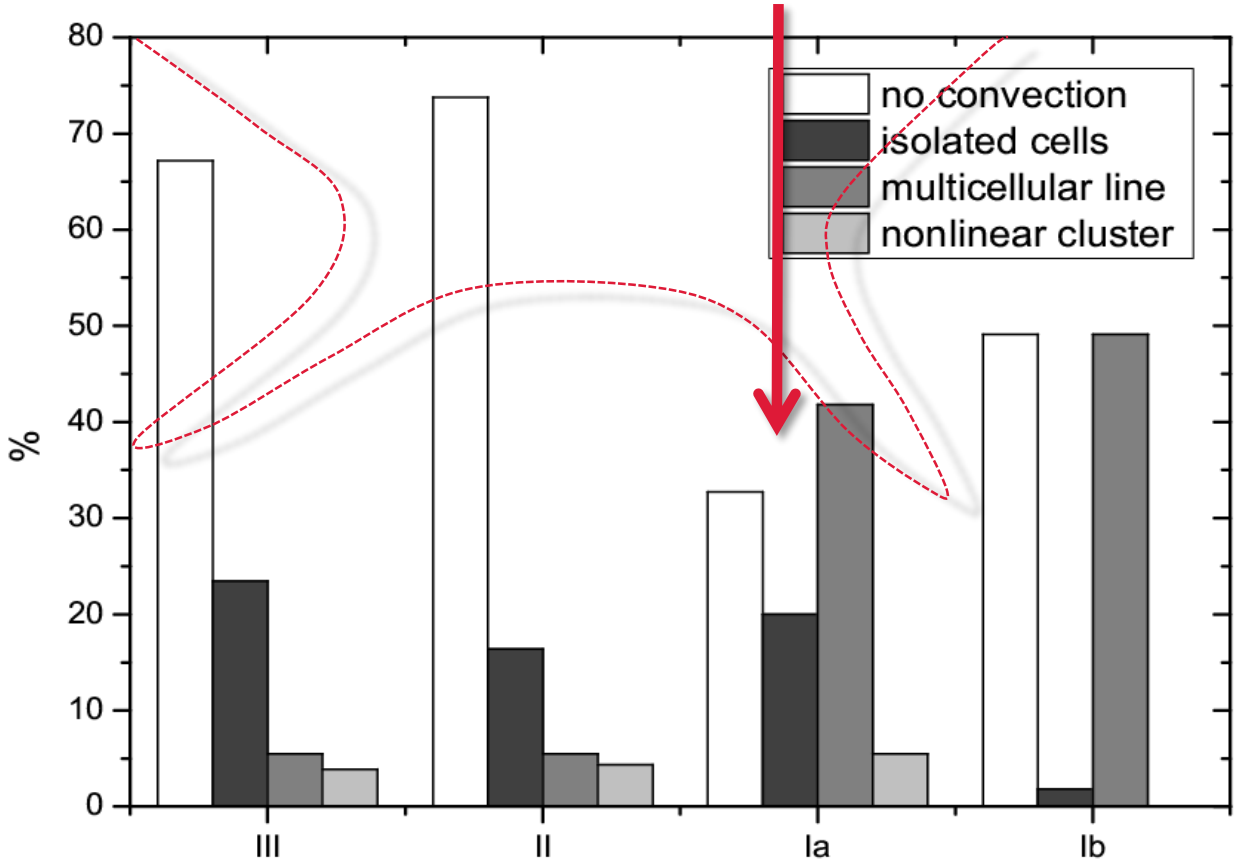

B. Antonescu, G. Vaughan, and D. M. Schultza. Five-year Radar-based climatology of tropopause folds and deep convection over Wales, United Kingdom, *Mon. Wea. Rev.*, 2013, 141,1693-1707.

4. Connection with hazard weather events

A case study:

Convective weather report during 06-12UTC 20 Jun 2022

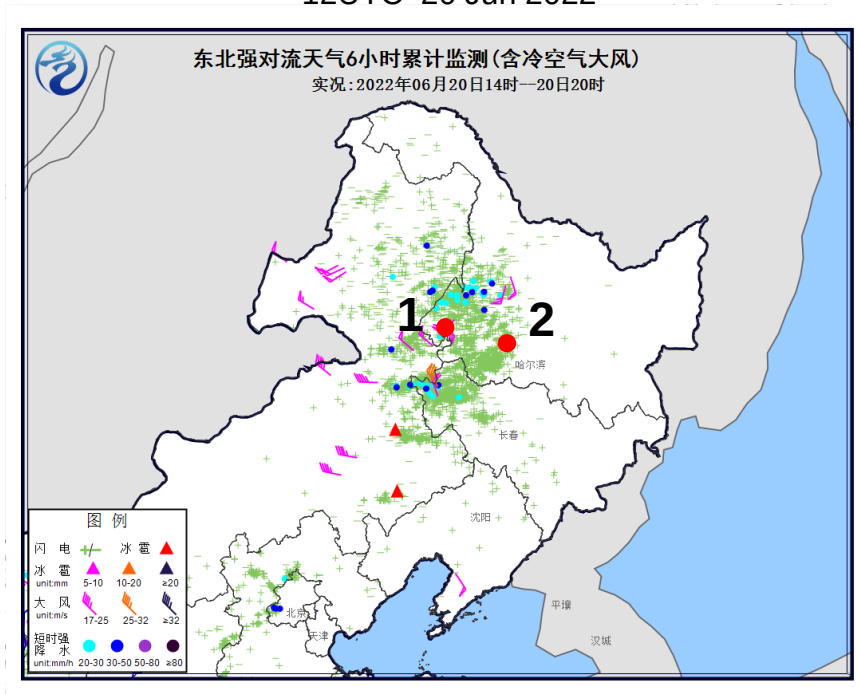

Table. The environmental parameters at Qiqi Haer(station 1) and Haer Bin (station 2) at 0000UTC and 1200UTC 20 June 2022.

St.	Name	MUCAPE(00UTC)	MUCAPE(12UTC)	Lapse rate $_{700\text{-}500hPa}$ (00UTC)	Lapse rate $_{700\text{-}500hPa}$ (12UTC)
1	Qiqi Haer	6	**804** ↑	6.3℃/km	**6.5℃/km** ↑
2	Haer Bin	67	**2160** ↑	5.8℃/km	**7.6℃/km** ↑

Station 1： Qiqi Haer

Jun 20 0000UTC

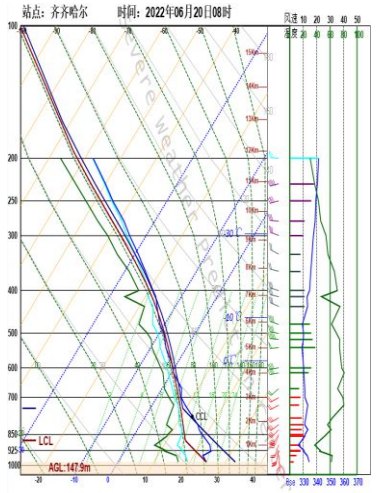

Jun 20 1200UTC

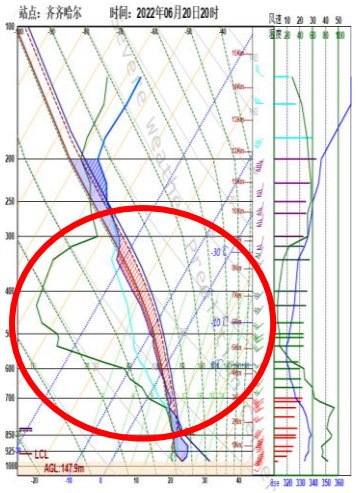

Station 2： Haer Bin

Jun 20 0000UTC

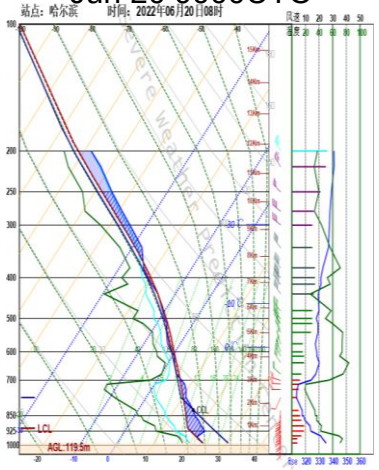

Jun 20 1200UTC

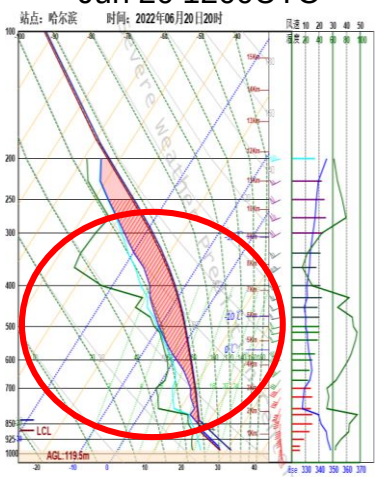

Figure. The T-lnp diagrams at Qiqi Haer (location 1 in the left figure) at 0000UTC and 1200UTC 20 June 2022

4. Connection with hazard weather events

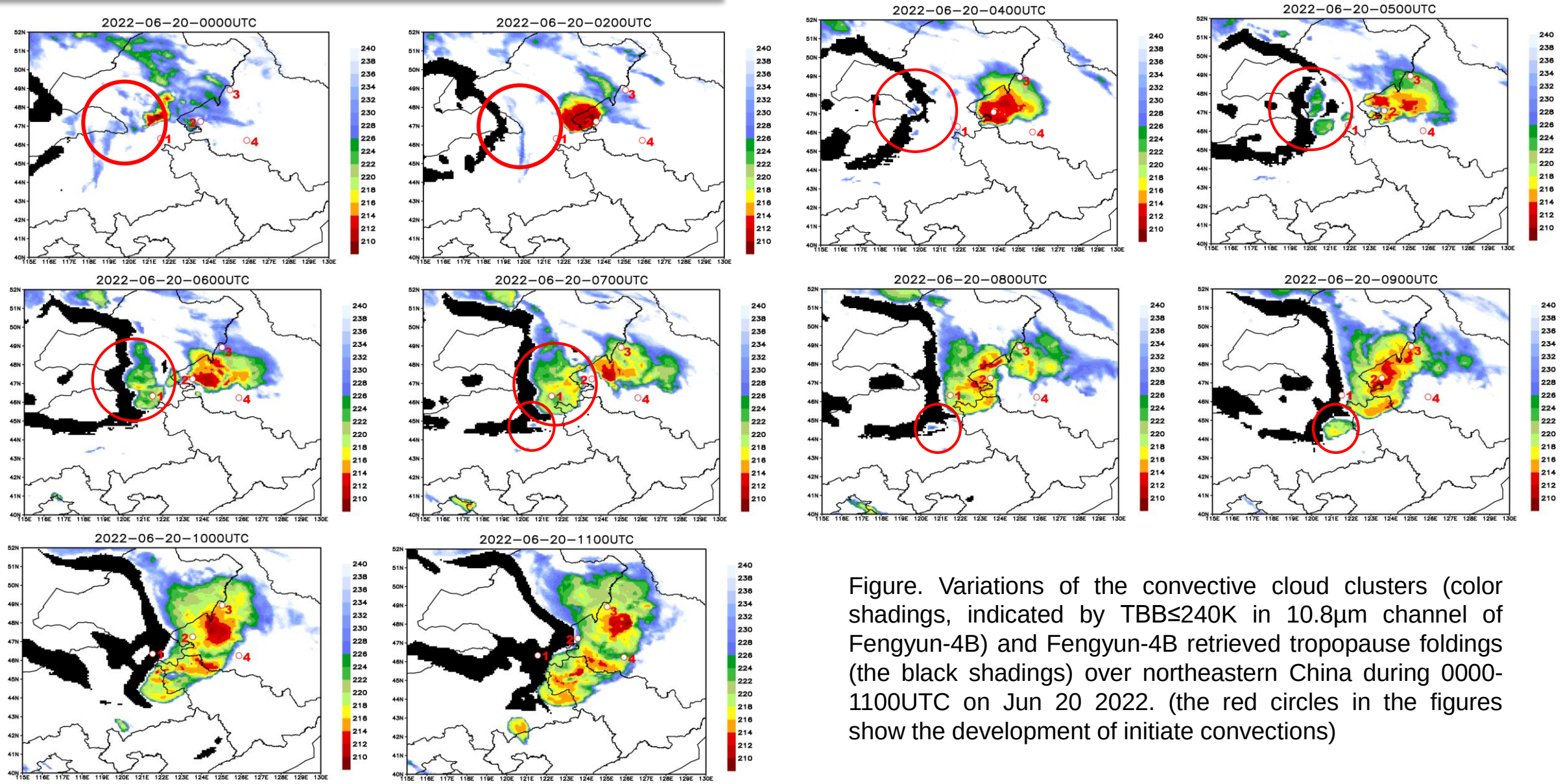

Figure. Variations of the convective cloud clusters (color shadings, indicated by TBB≤240K in 10.8μm channel of Fengyun-4B) and Fengyun-4B retrieved tropopause foldings (the black shadings) over northeastern China during 0000-1100UTC on Jun 20 2022. (the red circles in the figures show the development of initiate convections)

4. Connection with hazard weather events

➢ Indicate for the CAT (clear air turbulence)

Note：
EOL-AMDAR data is the generally-accepted worldwide term for automated weather reports from commercial aircraft. The temporal resolution of the dataset is 1hr. It includes meteorological observations and turbulence measurments (wind, temperature, humidity, pressure etc.) along flight path.

EOL-AMDAR records within FY-4B disc on 24 Jan 2022. (green dots)

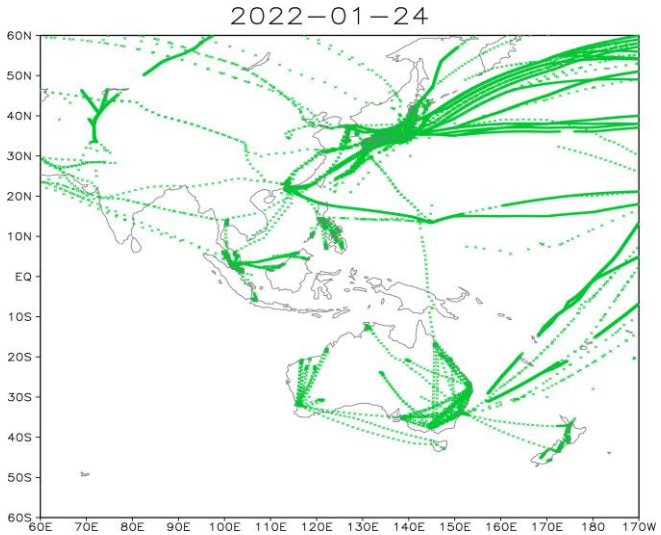

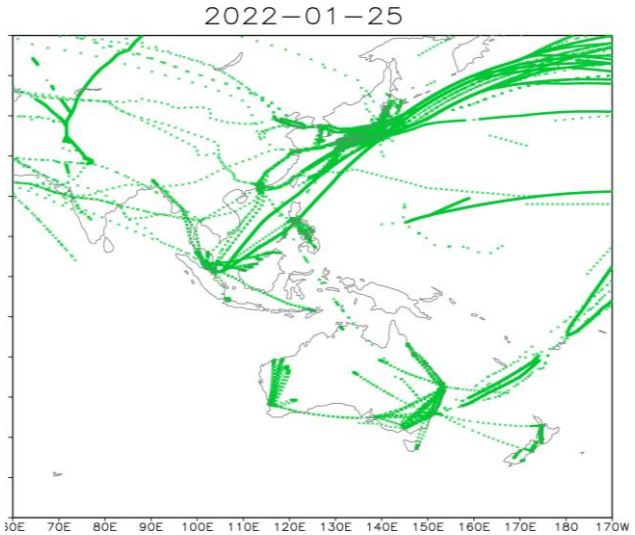

EOL-AMDAR records within FY-4B disc on 25 Jan 2022. (green dots)

EOL-AMDAR records having turbulence measurments, i.e. EDR values on 24 Jan 2022. (blue dots for EDR<0.1;orange dots for 0.1<EDR<0.22;red dots EDR>0.22)

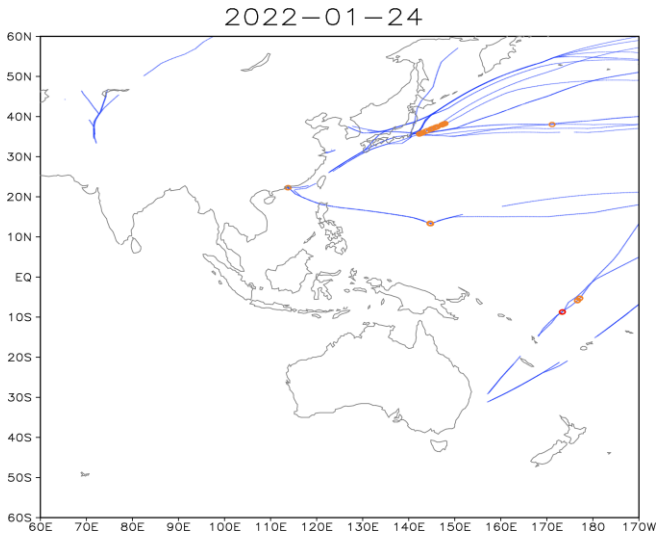

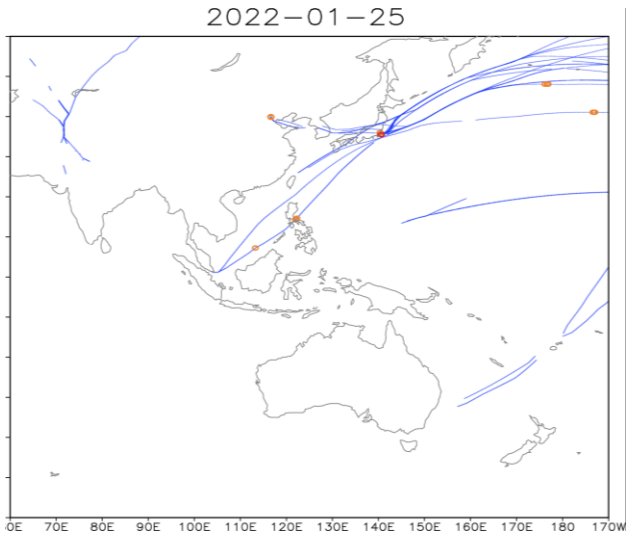

EOL-AMDAR records having turbulence measurments, i.e. EDR values on 25 Jan 2022. (blue dots for EDR<0.1;orange dots for 0.1<EDR<0.22;red dots EDR>0.22)

4. Connection with hazard weather events

To assess the potential application for using FY-4B tropopause foldings to indicate CAT, we select the EOL-AMDAR data which have EDR records and are observed above 5000m when flights fly in partly cloud areas to compare with tropopause foldings. Here, we use the similar methods for evaluating FY4B tropopause foldings precision to assess the assess the accuracy of FY-4B tropopause foldings as indicators of CAT. According to the preliminar results, the FY-4B tropopause foldings have **74%** accuracy for indicating light to moderate CAT.

Valid samples：13682

Table. International Civil Aviation Organization (ICAO) (2001)

Parameter	no turbulence	turbulence
EDR($\varepsilon^{1/3}(m^{2/3}s^{-1})$)	[0,0.1)	≧0.1

Table. Definition of the parameters used in the statistics

		FY-4B tropopause foldings as proxy of the clear air turbulence	
		Y (turbulence)	N (no turbulence)
EOL-AMDAR observations	Y (turbulence)	A(yy)	B(yn)
	N (no turbulence)	C(ny)	D(nn)

Table. Accuracy of FY-4B tropopause foldings as indicators of CAT (test time duration: 24-25 Jan 2022)

	FY4B tropopause foldings
HR	0.92
POD_turb	0.74
POD_unturb	0.92

$$POD\_turb = \frac{A}{A+B} \quad (1)$$

$$POD\_unturb = \frac{D}{C+D} \qquad POD \in [0,1], \quad (2)$$

$$HR = \frac{A+D}{A+B+C+D} \qquad HR \in [0,1], \quad (3)$$

4. Connection with hazard weather events

This is a case for using tropopause folding product to detect light to moderate turbulence occurred over Aurstralia on 22 Jan 2018.

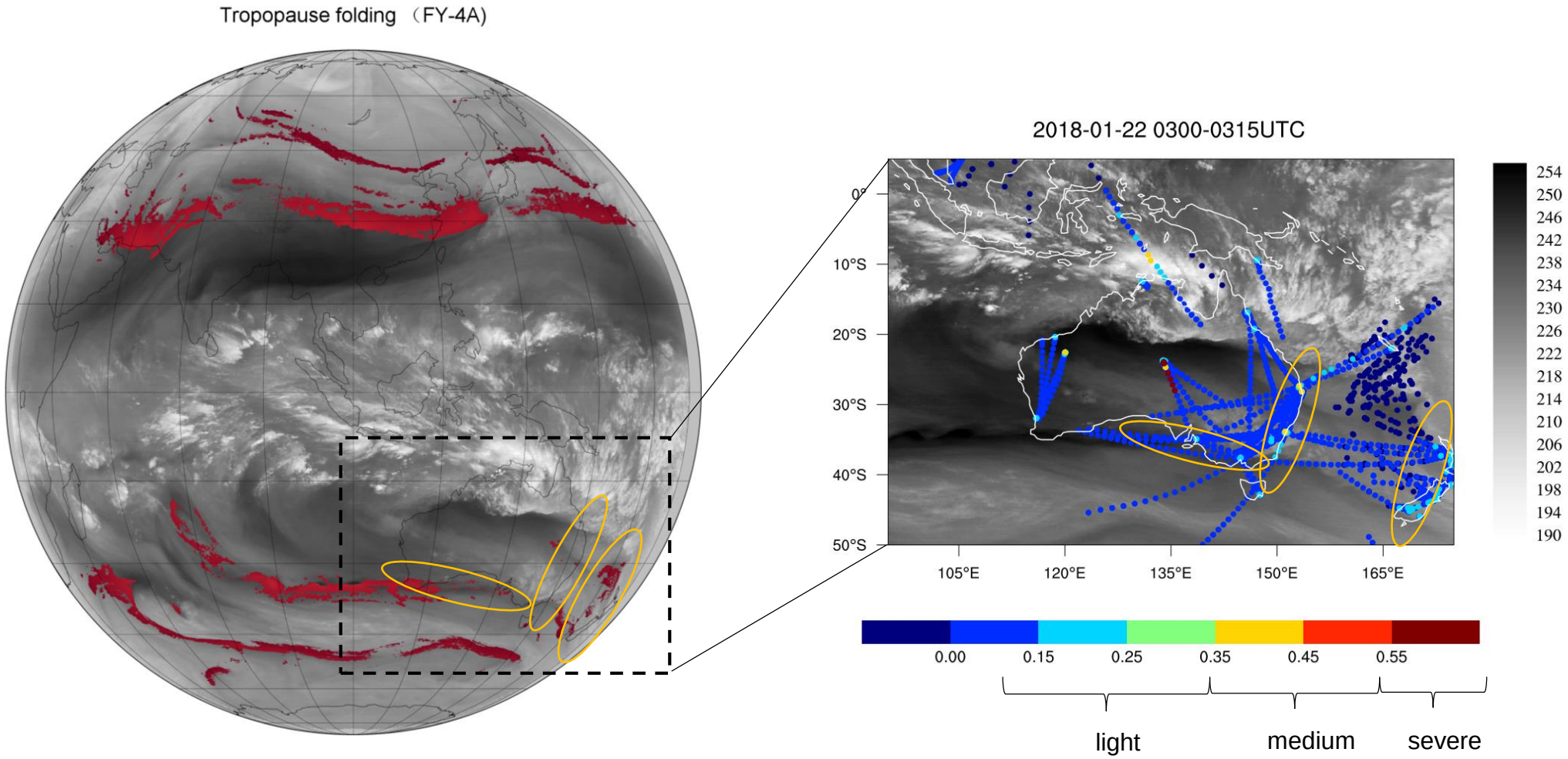

5. Summary

- By evaluating FY-4B tropopause foldings product against GEOS-5/MERRA-2 reanalysis, it suggests that the retrieved tropopause pressure has the RMSE of ~40hPa, standard deviation of ~30hPa, and correlation coefficient of ~0.9; while the retrieved tropopause temperature has the RMSE of ~6K, standard deviation of ~4K, and correlation coefficient of ~0.9. The accuracy of tropopause foldings is over 80%.

- Case studies show great potential benefit for convection applications.

- By evaluated with the aircraft in situ EDR (eddy dissipation rate) observations, the probability of detection turbulence by tropopause folds is ~ 0.7 which illustrate the potential correlation of tropopause folding with the clear-air turbulence at upper-level troposphere.

Thank you!

References

- Santurette, P., Georgiev C. G., 2005. Weather Analysis and Forecasting: Applying Satellite Water Vapor Imagery and Potential Vorticity Analysis. ISBN: 0-12-619262-6. Academic Press, Burlington, MA, San Diego, London. Copyright ©, Elsevier Inc. 179 pp.
- Browell, E.V. et al. (2003), Ozone, aerosol, potential vorticity, and trace gas trends observed at high-latitudes over North America from February to May 2000, J. Geophys.Res., 108(D4).
- Cho, J. Y. N., et al. (1999), Observations of convective and dynamical instabilities intropopause folds and their contribution to stratosphere-troposphere exchange, J.Geophys. Res., 104, 21,549-21,568, 1999.
- Cornman, L. B., P. Schaffner, C. A. Grainger, R. T. Neece, T. S. Daniels and J. J. Murray(2004), Eddy dissipation rate performance of the Tropospheric AirborneMeteorological Data Reporting (TAMDAR) sensor during the 2003 AtlanticTHORPEX regional campaign, AMS 11th conference on aviation, range and aerospace.
- Danielson, E. F. (1968), Stratospheric-tropospheric exchange based on radioactivity,ozone and potential vorticity. J. Atmos. Sci. 25, 502- 518.
- Gibbs, B. (2008) GOES image navigation and registration, SatMagazine, July 2008 Edition, http://www.satmagazine.com/cgi-bin/display_article.cgi?number=1889485593.
- Harbaugh, A.W., 1990, A simple contouring program for gridded data: U.S. Geological Survey Open-File Report 90-144, 37 p.
- Holton, J.R., P.H. Haynes, M.E. McIntyre, A.R. Douglass, R.B. Rood, and L. Pfister (1995), Stratosphere-Troposphere Exchange, Rev. Geophys., 33 (4), 403-439.
- Johnson, W.B., and W. Viezee (1981), Stratospheric ozone in the lower troposphere--I.Presentation and interpretation of aircraft measurements, Atmos. Environ., 15 (7), 1309-1323.
- Keyser, D., and M. J. Pecnick, (1985a), A two-dimensional primitive equation model offrontogenesis forced by confluence and horizontal shear. J. Atmos. Sci., 42, 1259-1282.
- Yang, J., Zhang, Z., Wei, C., Lu, F. and Guo, Q. (2017) Introducing the new generation of Chinese geostationary weather satellites, Fengyun-4. Bulletin of the American Meteorological Society, 98, 1637–1658.